



Structure and exhumation of the Cap des Trois Fourches basement rocks (Eastern Rif, Morocco)

A. Azdimousa, A. Jabaloy-Sánchez, P. Münch, J. M Martínez-Martínez, G. Booth-Rea, M. Vázquez-Vilchez, L. Asebriy, J. Bourgois, F. González-Lodeiro

► To cite this version:

A. Azdimousa, A. Jabaloy-Sánchez, P. Münch, J. M Martínez-Martínez, G. Booth-Rea, et al.. Structure and exhumation of the Cap des Trois Fourches basement rocks (Eastern Rif, Morocco). Journal of African Earth Sciences, 2018, 150, pp.657-672. 10.1016/j.jafrearsci.2018.09.018 . hal-01884964

HAL Id: hal-01884964

<https://hal.science/hal-01884964>

Submitted on 1 Oct 2018

HAL is a multi-disciplinary open access archive for the deposit and dissemination of scientific research documents, whether they are published or not. The documents may come from teaching and research institutions in France or abroad, or from public or private research centers.

L'archive ouverte pluridisciplinaire **HAL**, est destinée au dépôt et à la diffusion de documents scientifiques de niveau recherche, publiés ou non, émanant des établissements d'enseignement et de recherche français ou étrangers, des laboratoires publics ou privés.

Accepted Manuscript

Structure and exhumation of the Cap des Trois Fourches basement rocks (Eastern Rif, Morocco)

A. Azdimousa, A. Jabaloy-Sánchez, P. Münch, J.M. Martínez-Martínez, G. Booth-Rea, M. Vázquez-Vilchez, L. Asebriy, J. Bourgois, F. González-Lodeiro



PII: S1464-343X(18)30300-5

DOI: [10.1016/j.jafrearsci.2018.09.018](https://doi.org/10.1016/j.jafrearsci.2018.09.018)

Reference: AES 3330

To appear in: *Journal of African Earth Sciences*

Received Date: 30 January 2017

Revised Date: 31 August 2018

Accepted Date: 25 September 2018

Please cite this article as: Azdimousa, A., Jabaloy-Sánchez, A., Münch, P., Martínez-Martínez, J.M., Booth-Rea, G., Vázquez-Vilchez, M., Asebriy, L., Bourgois, J., González-Lodeiro, F., Structure and exhumation of the Cap des Trois Fourches basement rocks (Eastern Rif, Morocco), *Journal of African Earth Sciences* (2018), doi: <https://doi.org/10.1016/j.jafrearsci.2018.09.018>.

This is a PDF file of an unedited manuscript that has been accepted for publication. As a service to our customers we are providing this early version of the manuscript. The manuscript will undergo copyediting, typesetting, and review of the resulting proof before it is published in its final form. Please note that during the production process errors may be discovered which could affect the content, and all legal disclaimers that apply to the journal pertain.

1 **Structure and exhumation of the Cap des Trois Fourches basement rocks (Eastern
2 Rif, Morocco)**

3
4 Azdimousa, A.¹, Jabaloy-Sánchez, A.², Münch, P.³, Martínez-Martínez, J.M.^{2,4}, Booth-
5 Rea, G.^{2,4}, Vázquez-Vilchez, M.⁵, Asebriy, L.⁶, Bourgois, J.⁷, González-Lodeiro, F.⁸

6
7
8 1 Faculté Pluridisciplinaire de Nador & Laboratoire des Géosciences Appliquées, Faculté
9 des Sciences, Université Mohammed I, Oujda, Morocco.

10 2 Departamento de Geodinámica, Universidad de Granada, Granada, (Spain).

11 3 Géosciences Montpellier, Université de Montpellier, Campus Triolet CC060, place
12 Eugene Baitaillon, 34095 Montpellier cedex, France.

13 4 Instituto Andaluz de Ciencias de la Tierra, UGR-CSIC, Avda. de las Palmeras, 18100
14 Armilla, Granada, (Spain)

15 5 Departamento de Didáctica de las Ciencias Experimentales, Facultad de Ciencias de la
16 Educación, Universidad de Granada, Granada, Spain)

17 6 Institut Scientifique, B.P. 703, Université Mohammed V, Agdal-Rabat, Morocco.

18 7 Université Pierre et Marie Curie - Paris 6. Institut des Sciences de la Terre Paris (iSTeP)
19 - UMR 7193 UPMC-CNRS Case 124, Tour 46-00, 3 ème étage, 4, place Jussieu, 75252
20 Paris Cedex 5, France

21 8 Instituto Geológico y Minero de España, Ríos Rosas 23, 28003 Madrid, Spain

22
23
24
25
26
27
28
29
30

31 **Abstract**

32 The Cap des Trois Fourches (Eastern Rif, northern Morocco) metamorphic
33 basement exposes two major tectonic units, namely the Taïdant unit underthrusting the
34 overlying Tarjât tectonic unit. The Tarjât tectonic unit is composed of metamorphic rock
35 originating from detrital material. This upper Tarjât tectonic unit exhibits: (1) orthogneiss
36 bodies being Paleozoic in age and (2) evidences showing a retrograde metamorphism during the
37 Alpine orogenesis. U-Pb SHRIMP zircon geochronology from the orthogneiss bodies has
38 yielded Sakmarian (Early Permian) ages for the intrusion of their protoliths. The lower
39 Taïdant unit is formed of green and brown shales associated with quartzite beds. A
40 Mesozoic age is commonly accepted for this unit.

41 The internal structure of the Tarjât tectonic unit consists in km-scale folds trending
 42 ENE-WSW with an up-dip direction towards the SE. This compressional deformational
 43 stage was superimposed on internal thrust sheets controlled by ductile shear zones with a
 44 SW-vergent transport sense. The lower Taïdant unit shows conspicuous bedding associated
 45 with a penetrative foliation outlining a monocline structure dipping gently towards the
 46 NW. The major ductile-brittle detachment fault bounding the upper Tarjât tectonic unit
 47 from the lower Taïdant unit –i.e. the local basement– exhibits evidences for a top-to-the-
 48 west sense of motion. We assume that this specific fault is the prolongation into the Cap
 49 des Trois Fourches area of the extensional detachment previously described in the
 50 Temsamane area. Therefore, this low angle detachment fault is a major tectonic element
 51 extending hundreds of km through the Eastern Rif. We postulate that this major
 52 detachment roots deep in the Eastern Rif basement. This detachment is cut at the surface
 53 by the Nekor normal-sinistral strike-slip fault that separates thin 24-32 km thick
 54 metamorphic Eastern Rif crust from the 50-55 km thick crust of the western Rif. This
 55 transtensive fault system exhumes the Rif middle crust, represented by the Temsamane
 56 massif units, along the Nekor sinistral STEP boundary at the southern edge of the Betic-Rif
 57 subduction system.

58

59 **Keywords:** Rif Chain, Cap des Trois Fourches, ductile-brittle detachment fault, U-Pb
 60 SHRIMP zircon geochronology

61

62 1. - Introduction

63 The Eastern Rif Chain (Northwest Africa, Fig. 1) is characterized by very low- to
 64 low-grade metamorphic terranes derived from the Mesozoic Maghrebian palaeomargin
 65 cropping out in different isolated sectors along the Mediterranean coast (Frizon de

66 Lamotte, 1985; Frizon de Lamotte et al., 1991; Azdimousa et al., 2007; Chalouan et al.,
67 2008; Jabaloy et al., 2015). It notably includes the Temsamane area, the Cap des Trois
68 Fourches and the Khebaba massif (Frizon de Lamotte, 1985; Frizon de Lamotte et al.,
69 1991; Azdimousa et al., 2007; Negro et al., 2008; Booth-Rea et al., 2012; Jabaloy et al.,
70 2015) (Figs. 1 and 2). The sequences of these areas include metapelitic Paleozoic rocks
71 covered by Triassic greenschists and Jurassic to early Cretaceous marbles and metapelites
72 (Frizon de Lamotte, 1985; Frizon de Lamotte et al., 1991; Azdimousa et al., 2007; Negro et
73 al., 2008; Booth-Rea et al., 2012; Jabaloy et al., 2015). Those rocks are characterized by
74 LT-IP Alpine metamorphic conditions (Negro, 2005; Negro et al., 2007; Jabaloy et al.,
75 2015), and by penetrative Alpine ductile deformations. Most of the rocks also were
76 exhumed by a ductile-brittle extensional detachment (see Azdimousa et al., 2007; Booth-
77 Rea et al. 2012; Jabaloy et al., 2015). At the present day, those metamorphic outcrops are
78 isolated, making their mutual correlation difficult to disentangle the first order structure of
79 the area that is a basic key point to understand the evolution of the North Africa
80 palaeomargin.

81 One of the aforementioned outcrops occurs in the Cap des Trois Fourches sector
82 (Figs. 2 and 3), where scarce detailed studies have been performed (Guillemin et al., 1983;
83 García-Dueñas et al., 1995; Sánchez-Gómez, 1996; Michard et al., 2008; Negro et al.,
84 2008). The rocks of this specific massif have been tentatively correlated with those of the
85 Internal Rif (García-Dueñas et al., 1995; Sánchez-Gómez, 1996) or the uppermost and
86 most metamorphosed of the Temsamane metamorphic units: the Ras Afraou unit (Michard
87 et al., 2008; Negro et al., 2008).

88 Our main aim is to establish the structure of the low-grade metamorphic outcrops of
89 the Cap des Trois Fourches sector in order to determine their tectonic evolution and
90 correlation with the Rifian structures. In order to do so we carried a detailed microtectonic

91 analysis combined with $^{40}\text{Ar}/^{39}\text{Ar}$ ages on white micas and SHRIMP U-Pb dating on
 92 zircons.

93

94 **2.-Tectonic setting**

95 The Rif Chain is an Alpine mountain belt bordering northern Morocco (Fig. 1) that
 96 in union with the Betic Chain belt in southern Spain form the Betic–Rif orogen (e.g.,
 97 Booth-Rea et al., 2005; Chalouan et al., 2008; Platt et al., 2013, and references therein).
 98 This orogen was formed during the westward drifting of the Alborán domain (Andrieux et
 99 al., 1971; Bourgois, 1977; Balanyá and García-Dueñas, 1987), at the same time as the
 100 African and Eurasian plates converged (e.g., Chalouan and Michard, 2004; Jolivet et al.,
 101 2003) during the Oligocene-Miocene times (Chalouan and Michard, 2004; Chalouan et al.,
 102 2008).

103 The tectonic model for these movements in the Western Mediterranean area is
 104 controversial, although most of them involve the westwards roll back of a SE-dipping slab
 105 of Tethys lithosphere below the Alborán domain (i.e. Rosenbaum et al., 2002; Faccenna et
 106 al., 2004; Booth-Rea et al., 2007; Carminati et al., 2012; Chertova et al., 2014), while
 107 others authors propose delamination or convective removal of the subcontinental mantle
 108 lithosphere (Calvert et al., 2000; Platt et al., 1998; Seber et al., 1996). Seismic studies have
 109 delimited a SE-dipping high-velocity slab within the upper mantle beneath the Gibraltar
 110 Arc (i.e. Bezada et al., 2013; Palomeras et al., 2014; Thurner et al., 2014; Mancilla et al.,
 111 2015; Villaseñor et al., 2015) that together with geochemical data of volcanic rocks in the
 112 region (Duggen et al., 2008; Varas-Reus et al., 2017) and the volcanic arc structure of the
 113 East Alboran basin (Booth-Rea et al., in press) favours the subduction/roll-back models.
 114 However, delamination of the subcontinental lithosphere at the edges of the subduction
 115 system in the Betics and Rif, coeval to slab rollback, is supported by the geochemical

116 evolution of volcanism (Duggen et al., 2003), by tectonic analysis (Martínez-Martínez et
117 al., 2006), and by receiver function data that show a missing orogenic root under parts of
118 the Betics and the Eastern Rif (Thurner et al., 2014; Mancilla et al., 2015). Delamination
119 occurred under the continental orogenic crust inboard of Subduction Transfer Edge
120 Propagator boundaries (STEP, Govers and Wortel, 2005) at the northern and southern
121 edges of the Betic-Rif orogen (Mancilla et al., 2015).

122 From the Mediterranean coast towards the south, three main structural domains
123 compose the Rif belt (Fig. 1):

- 124 i) Internal Rif or Alborán Domain that is an allochthonous terrain mainly
125 composed by metamorphic and sedimentary rocks exhibiting ages ranging
126 from Paleozoic to Paleogene.
- 127 ii) Maghrebian Flysch units thrusted southward as tectonic sheets mainly
128 formed of Mesozoic-Cenozoic turbidites. They are commonly interpreted as
129 rocks originating from the main suture of the Tethys Ocean (Durand-Delga
130 et al., 2000). Bourgois (1980 a, b) has inferred that this main suture is
131 located north of the Internal Zones in the Betic Chain.
- 132 iii) External Rif formed of Mesozoic to Cenozoic sediments and
133 metasediments, and interpreted as the North African passive margin of the
134 Tethys Ocean.

135 Traditionally, the External Rif rocks have been grouped into three main zones: the
136 Prerif, the Intrarif, and the Mesorif zones (Suter, 1980a, b). The Prerif zone is the
137 outermost zone of the External Rif and is located to the south. It comprises a frontal fold-
138 and-thrust belt that deforms thin Jurassic and Lower Cretaceous successions detached from
139 the Paleozoic basement of the Variscan Western Moroccan Meseta (“Rides Prérifaines”,
140 see Michard, 1976; Ben Yaïch, 1991; Favre, 1992). The “Rides Prérifaines” are overlain

141 by an olistostromic complex formed of Paleozoic to Cenozoic blocks in a matrix of
 142 Tortonian marls (“Nappe Préfaine”, Levy and Tilloy, 1952; Vidal, 1971; Leblanc, 1975-
 143 1979; Bourgois, 1977; Suter, 1980a, b; Feinberg, 1986; Kerzazi, 1994).

144 The Mesorif zone is formed of allochthonous units with Triassic to Paleogene
 145 successions thrusting over autochthonous or para-autochthonous successions culminating
 146 with Middle-Upper Miocene turbidites and olistostromes. Those lithological successions
 147 are thought to be deposited in proximal areas of the African paleomargin (e.g. Chalouan et
 148 al., 2008). However, recently Benzaggagh et al. (2014) have proposed the existence of
 149 ophiolitic massifs indicating the opening of ocean-floor basins within the Mesorif domain.
 150 In the eastern Rif, those Mesorif units correspond to the Temsamane units that underwent
 151 ductile deformations and IP-IT metamorphism during Alpine times (see Azdimousa et al.,
 152 2007, Jabaloy et al., 2015, and references therein).

153 The Intrarif zone includes the distal units derived from the African paleomargin.
 154 These units crop out immediately beneath the Maghrebian Flyschs and Internal Rif and are
 155 characterized by a thick accumulation of sediments with ages ranging from Lower Jurassic
 156 to Cretaceous. These sediments underwent ductile deformations that developed under
 157 diagenetic to anchizone conditions (Andrieux, 1971; Asebriy, 1994; Asebriy et al., 2003;
 158 Azdimousa et al., 1998, 2003, 2007; Vazquez et al., 2013). The Mesorif units include the
 159 Ketama unit, overlain by the partly detached Tanger unit, and the Aknoul nappe, totally
 160 detached and containing the Upper Cretaceous-Eocene succession.

161 Asebriy et al. (1987) have defined the Subrif zone located north of the Prerif zone
 162 that includes the Intrarif and Mesorif units as defined by Durand-Delga et al. (1962) and
 163 (Suter, 1980a,b). In the Eastern Rif (Fig. 2), the External Rif includes three main sets of
 164 tectonic units. From bottom to top, it includes: the Temsamane fold-and-thrust stack, the
 165 Tanger-Ketama unit, and the Aknoul unit.

166 The lithological sequence of the Temsamane fold-and-thrust stack begins with dark
 167 Paleozoic schists covered by Triassic greenschists and Jurassic marbles. Continuing up
 168 section, whitish Berriasian–Barremian phyllites and shales alternate with marbles, and they
 169 are covered by dark Aptian–Early Albian phyllites and shales alternating with quartzites
 170 (Frizon de Lamotte, 1985; Frizon de Lamotte et al. 1991; Azdimousa et al., 2007). The
 171 rocks are deformed by isoclinal to tight folds with N70°E strikes and SSE vergences (see
 172 Azdimousa et al., 2007; Jabaloy et al., 2015). Ductile shear zones bound several fold-
 173 nappes (Jabaloy et al., 2015). The metamorphic P-T conditions increase towards the NW,
 174 with late diagenesis reaching epizone at chlorite–illite conditions in the lowermost fold-
 175 nappe. The early Cretaceous metapelites in the intermediate Temsamane fold-nappes, and
 176 the Paleozoic schists in both the Ras Afraou and Khebaba units at the top of the stack,
 177 exhibit chloritoid bearing facies (Frizon de Lamotte, 1987; Negro, 2005; Negro et al.,
 178 2007).

179 Negro (2005), Negro et al. (2007), Jabaloy et al. (2015), have estimated the PT
 180 metamorphic conditions of the rocks in the uppermost Temsamane unit (Ras Afraou unit)
 181 at 7–8 kbars and 350 ± 30 °C. $^{40}\text{Ar}/^{39}\text{Ar}$ radiometric analyses on white micas have yielded
 182 ages ranging from 23 to 8 Ma (Monié et al., 1984; Negro et al., 2008; Jabaloy et al., 2015).
 183 Negro et al. (2008) and Jabaloy et al. (2015) have proposed the older Oligocene ages
 184 correspond to the metamorphic peak during subduction, and those of the Middle to Late
 185 Miocene date the cooling during extensional exhumation of the rocks.

186 The exhumation of the Temsamane metamorphic rocks took place along a major
 187 extensional detachment with tectonic transport towards the WSW that is the so-called
 188 Temsamane detachment, separating the Temsamane fold-and-thrust stack in the footwall
 189 from the Tanger–Ketama and Aknoul units in the hanging wall (Booth-Rea et al., 2012). In
 190 turn, the sedimentary Mesozoic cover of the Eastern Moroccan Meseta or their

191 prolongation as the Middle Atlas underthrusts the metamorphic Temsamane fold-and-
 192 thrust stack. In contrast, the structure in the western Rif includes structurally higher rock
 193 units with the thick Jurassic marbles and Cretaceous slates of the Tanger-Ketama unit (see
 194 Vázquez et al., 2013) covering the ophiolitic bodies of the Central Rif (Benzaggagh et al.,
 195 2014; Amar et al., 2015), and, in turn, these rocks are overthrust by the Maghrebian Flysch
 196 units and the Internal Rif Alboran domain rocks.

197 Below the Rif Chain, the Moho shows strong differences in depth, ranging from
 198 more than 50 km below the western and central Rif to around 24 km below the eastern Rif.
 199 These two structural domains are separated by a steep transition zone (Mancilla et al.,
 200 2012, 2015; Díaz et al., 2016) located beneath the active Trougout-Nekor Fault-system.
 201 GPS data (Vernant et al., 2010; Pérouse et al. 2010) and reorganization of the drainage
 202 networks (Barcos et al., 2014) have recorded the tectonic activity along this Trougout-
 203 Nekor fault system. This sinistral transtensional fault-system (Asebriy et al., 1993; Barcos
 204 et al., 2014; Poujol et al., 2014) accommodates most of the Present-day Western Rif belt
 205 displacement towards the WSW with respect to the stable Nubia (Poujol et al., 2014).

206

207 **3. - Geology of the Cap des Trois Fourches area**

208 The rocks of the Cap des Trois Fourches area extend along the Peninsula of Melilla,
 209 a North-South elongated cap on the southern border of the Alboran Sea (northeast of
 210 Morocco, Figs. 2 and 3) in an open antiform striking NE-SW: the Tarjât (also known as
 211 Taryat) anticline (Guillemin and Houzay, 1982). The normal left-handed Aït Lahsene fault
 212 bounds the NW limb of the Tarjât anticline (Ait Brahim, 1991; Morel, 1988; Azdimousa et
 213 Bourgois, 1993). García-Dueñas et al. (1995) and Michard et al., (2007) have recognized
 214 two tectonic units in the area:

215 i.- The Tarjât Unit (García-Dueñas et al., 1995) formed of chloritoid-bearing
 216 schists, phyllites, quartzites and marbles that underwent MP-LT metamorphism at around
 217 7-9 kbars and 330-430 °C during the Oligocene times (Negro et al., 2007, 2008). This unit
 218 overlies a detachment underlined by fragments of chloritites and “serpentinites” (García-
 219 Dueñas et al., 1995; Michard et al., 2007) that separates it from

220 ii.-the Taïdant Unit (García-Dueñas et al., 1995) formed of a thin sequence of
 221 shales and greywackes attributed to the Carboniferous.

222 García-Dueñas et al. (1995), and Negro et al. (2007, 2008) have previously
 223 described the grey chloritoid-bearing micaschists. These micaschists exhibit mineral
 224 associations including chlorite + phengite + quartz ± chloritoid ± paragonite ± kaolinite.
 225 The XMg from chloritoid shows values varying between: 0.08-0.14 (see Negro et al.,
 226 2007). They document 7-9 kbars and 330-430 °C metamorphic P-T conditions for the grey
 227 schists at the base of the Tarjât unit. Also, they provide evidences for this metamorphism
 228 occurring during the Oligocene. The presence of kaolinite substantiates a
 229 retrometamorphic event that occurred during the late Miocene times. The previous studies
 230 of the metamorphic rocks discuss if they can be ascribed to the foreland of the Rif Chain
 231 (the Eastern Moroccan Meseta, Fernandez Navarro, 1911; Suter, 1980), to the Mesorif
 232 zone as the continuation of the outcrops of the Temsamane unit (Azdimousa et al., 2007;
 233 Michard et al., 2007; Booth-Rea et al., 2012), or to the Internal Rif (García-Dueñas et al.,
 234 1995; Negro et al., 2008).

235 Late Tortonian to Messinian sediments and volcanoclastics rocks, detached from
 236 the underlying metamorphic basement, crop out in the central part of the Melilla peninsula
 237 forming the Melilla Neogene basin (i.e. see Roger et al., 2000; Münch et al., 2001 and
 238 2006 van Assen et al., 2006; and references therein). The northern and southern tips of the
 239 peninsula show two volcanic complexes. The northern Cap des Trois Fourches volcanic

240 field exhibits rhyolites and rhyodacites with Tortonian ages (9.8 ± 3 Ma; Hernandez and
 241 Bellon, 1985). The southern Gourougou stratovolcano composed of Si-K rich igneous
 242 rocks spatially associated with Si-poor, Na-rich lavas was active from 6.69 to 3.37 Ma
 243 (Duggen et al., 2005).

244

245 **4.-Description of rocks**

246 Analytical methods for separation of minerals, chemical analysis, X-ray diffraction
 247 (XRD), $^{40}\text{Ar}/^{39}\text{Ar}$ dating on white micas, and SHRIMP U-Pb on zircons are described in
 248 the supporting information. The field work in the Cap des Trois Fourches area has revealed
 249 the presence of a major ductile fault separating the Tarjât Unit (García-Dueñas et al., 1995)
 250 from the underlying Taïdant tectonic unit formed of very low-grade metamorphic rocks
 251 and essentially outcropping at the south-eastern part of the massif.

252

253 *4.1.- Stratigraphy of the Tarjât and the Taïdant unit*

254 The stratigraphic sequence of the Tarjât unit begins with more than 350 m of grey
 255 chloritoid-bearing micaschists interlayered with quartzite layers including orthogneiss
 256 bodies, first described in this work.

257 Orthogneiss bodies outcrop in the northern part of the massif near the road to the
 258 lighthouse (Figs. 3, 4 and 5A). These are metric lens-shaped bodies several decimetres in
 259 thickness. These orthogneiss bodies show borders paralleling the main schistosity of the
 260 chloritoid-bearing schists. White layers rich in felsic minerals alternating with light grey
 261 layers of white mica and biotite (Fig. 5B) define prominent layering. K feldspar is clearly
 262 visible as centimetric porphyroblasts surrounded by the layering (Fig. 5B). The main
 263 mineral association includes K feldspar + quartz + muscovite + biotite + rutile.

264 The sequence follows up section with a ~10 meters thick quartzite-micaschist
 265 package covered by a brecciated dolomitised yellow marble discontinuous level. This
 266 marble always shows overlapping contacts over the above described sequence. The
 267 serpentinite bodies previously described in the area (see García-Dueñas et al., 1995;
 268 Michard et al., 2007) have been found to be chlorite-rich rocks (chloritites according to
 269 Michard et al., 2007). XRD data in sample CTF2 shows the presence of chlorite and quartz
 270 (Fig. 6). No serpentine mineral group exist in the bulk XRD patterns. If they exist, the
 271 abundance of serpentine mineral is less than 1%. Chlorite is the main phyllosilicate
 272 component identified from its characteristic reflections (14.18 Å, 7.08 Å, 4.72 Å and 3.54
 273 Å) that differ from reflections of serpentine minerals (7.29 Å, 4.52 Å and 3.65 Å).

274 The lithological sequence of the underlying Taïdant Unit (García-Dueñas et al.,
 275 1995) consists of ~300 meters of green and brown shales interlayered with centimetric to
 276 decimetric levels of quartzites.

277
 278 *4.2.- Geochronology*

279 Two samples from the orthogneiss bodies have been collected (AP3-F, C3F; see
 280 Fig. 3 for location). Samples were divided into two parts. The first one has been used for
 281 major, trace elements and isotopes contents analyses, while the second fraction was used to
 282 extract zircons using standard separation techniques. The content in major elements (Table
 283 1S in Supplementary material) are as follow: $\text{SiO}_2 \approx 67\text{-}75$ wt %, $\text{Na}_2\text{O} + \text{K}_2\text{O} \approx 7\text{-}8$ wt %,
 284 low contents in $\text{MgO} \approx 0.14\text{-}0.24$ wt %, high $\text{Al}_2\text{O}_3 \approx 14.7\text{-}19.7$ wt %. Their protoliths are
 285 peraluminous granitoids ($\text{ASI} \approx 1.1\text{-}1.2$) (Fig. 5C, D, E and F). In silicate Earth-normalised
 286 diagrams they have negative anomalies in Ba, Nb, Sr, Zr, and Ti, and positive anomalies in
 287 U, Ta, Pb, and P (Fig. 7; Table 1S in Supplementary material). These rocks have low
 288 contents in REE, and also have chondrite-normalised enrichment in LREE relative to

289 HREE with negative Eu anomalies (Fig. 8; Table 1S in Supplementary material). The
 290 rocks also have low values of $^{87}\text{Rb}/^{86}\text{Sr}$ that are 3.002 and 10.241 with values of $^{87}\text{Sr}/^{86}\text{Sr}$
 291 of 0.707600 and 0.729318, being $^{87}\text{Sr}/^{86}\text{Sr}_{335\text{ Ma}}$ of 0.680488 and 0.693285. The values of
 292 $^{147}\text{Sm}/^{144}\text{Nd}$ are 0.166 and 0.169, with $^{143}\text{Nd}/^{144}\text{Nd}$ values of 0.512401 and 0.512369, being
 293 the $\epsilon\text{Nd}_{335\text{Ma}}$ of -3.-3 and -4.1 with a $T_{\text{DM(Ga)}}$ of 2.0 and 2.2 (see Table 1S in Supplementary
 294 material).

295 Sample AP3-F consists of a leucocratic mylonitised augengneiss. Zircons are
 296 abundant and euhedral to subhedral bipyramidal prisms with dimensions about 250 to
 297 100 μm (Fig. 8A). Most are brownish translucent crystals. Cathodoluminescence imaging
 298 reveals partial metamictic alteration of several of the small zircons. Well-defined
 299 oscillatory zoning can be imaged in most of the grains. U-Pb measurements on 31 different
 300 crystals yielded moderate to large concentrations of U (427.0-5869.4ppm) and Th (54.0-
 301 489.0ppm) with Th/U = 0.06-0.50 (Table 2S in Supplementary material). The data define a
 302 discordia by Pb loss and common Pb with an upper intercept at 271.2 +17.7 -18.8 Ma, and
 303 a lower intercept at -13.1 +105.4 -13.1 Ma (MSWD = 2.0913) (Fig. 8B). The 8 data with a
 304 higher age and more concordance yield a $^{206}\text{Pb}/^{238}\text{U}$ Age = 295 ± 4 Ma (mswd= 1.75) (Fig.
 305 8C).

306 Sample C3F consists of a white mylonitised augengneiss (see Fig. 5B) with
 307 centimetric K feldspar porphyroblasts with σ -structures. Zircons are abundant and euhedral
 308 to subhedral bipyramidal prisms with dimensions about 250 to 80 μm of major length and
 309 100 to 50 μm width. Most are brownish translucent crystals. Cathodoluminescence imaging
 310 reveals partial metamictic alteration of most of the small zircons and fracture patterns in
 311 several crystals; however, well-defined oscillatory zoning can be imaged in several grains
 312 (Fig. 8D). U-Pb measurements on 26 different crystals without metamictic alteration
 313 yielded moderate to large concentrations of U (349.5-4142.9 ppm) and Th (67.6-902.9

314 ppm) with Th/U = 0.05-0.62 (Table 3S in Supplementary material). The data define also a
 315 discordia by Pb loss and common Pb²⁰⁴ (Fig. 8E). The 11 analysis with higher and more
 316 concordant ages yield a ²⁰⁶Pb/²³⁸U Age = 290 ± 5 Ma (mswd= 4.32). All the previous data
 317 point to a Sakmarian (early Permian) age for the intrusion of the protoliths of the gneisses.

318 ⁴⁰Ar/³⁹Ar determinations in micro-populations (2 to 3 grains) of white mica in
 319 mylonitized porphyroclasts from the sample AP3-F (Fig. 8F) yield four disturbed spectra
 320 with individual total fusion ages between 195.23 ± 0.77 Ma and 205.88 ± 1.52 Ma (Fig. 9,
 321 Tables 4S to 7S in Supplementary material) and a weighted mean age of 202.45 ± 0.98 Ma.
 322 In one replica, we obtained a mini-plateau age with most of released Argon on one step,
 323 corresponding to 47% of ³⁹Ar, of 205.49 ± 1.49 Ma concordant with the total fusion age
 324 (205.88 ± 1.52 Ma) (Fig. 9A), and the weighted mean age calculated with all total fusion
 325 ages. For all the spectra, the age changes with constant Ca/K, suggesting Ar loss from a
 326 homogeneous population (e.g. Negro et al., 2008).

327

328 **5. Structure**

329

330 The different tectonic units of the area are separated by a major ductile shear zone
 331 roughly striking NE-SW that bounds the upper Tarjât unit from the underlying Taïdant
 332 unit. The shear zone is gently dipping towards the NW or NNW. This main ductile shear
 333 zone is nicely exposed just below a long section of the road to the lighthouse (Figs. 3 and
 334 4). The main surface is always marked by an iron-bearing carbonate mylonite. The
 335 mylonite has a very well defined stretching lineation (L_p , Fig. 10A) with trends varying
 336 between N50°E and N80°E and small dips gently dipping as undulating towards the NE
 337 and the SW. The S-C ductile structures related to the major shear zone document a top-to-
 338 the-WSW sense of movement (Fig. 10B).

339 A S_c crenulation cleavage (Fig. 10D) associated to a NE-SW trending antiform
 340 exhibiting a SE-vergence is bending the main fabric of the upper Tarjât unit (Fig. 10D).
 341 The reverse limb of the antiform is also cut and duplicated by another ductile shear zone
 342 striking N50°E that dips 30 to 40° towards the NW (Fig. 10C). This shear zone is also
 343 underlined by an iron-bearing carbonate mylonite, nicely exposed near the 403 m summit
 344 (Fig. 10D and E). The main fabric of the schists is a planar-linear fabric (S_p/L_p) with a
 345 schistosity (S_p) and a N50 to N80°E trending stretching lineation (L_p) (Figs. 10 F and G).
 346 Ductile S-C and S-C' structures within the schists and gneisses and asymmetric σ -
 347 structures around K feldspar porphyroblasts in the gneisses indicate deformation in a
 348 simple shear regime with a SW transport sense.

349 The lower Taïdant unit exhibits a slaty cleavage with N50°E strike and dips towards
 350 the NW. A pervasive crenulation with an axis trending around N20°E (Fig. 11) is warping
 351 the previous penetrative deformation.

352 The whole structure of the Tarjât and Taïdant units is tectonically superposed over
 353 the more metamorphic Tarjât unit by a major ductile-brittle horizontal fault near the sea
 354 level (Figs. 3, 4 and 12A). The main surface is marked downwards by brittle fault rocks:
 355 fault gauges and carbonated fault breccias (Figs. 12A and B). The striations measured in
 356 the fault zone at the base of the unit have NE-SW trends and subhorizontal dips.
 357 Cataclastic structures such as S-C structures and crushed clast trails indicate a SW sense of
 358 movement of the hanging wall.

359 Three major faults bound the horst exhibiting the metamorphic basement of the Cap
 360 des Trois Fourches area. It includes the Aït Lahsene Fault, the Râs Izemrân Fault, and the
 361 Mersa Taïdant Fault, clockwise (ALF, RIF, and MTF, respectively in Fig. 3).

362 Towards the northwest, there is the Aït Lahsene Fault, with N50°E strike and dip of
 363 60° toward the NW (Fig. 3). The Fault exhibits two sets of superimposed striations, one

364 horizontal and a latter one parallel the maximum dip line of the fault. The brittle structures
 365 on the fault surface indicate a former left-handed strike-slip sense of movement coeval
 366 with of the opening of the Cap des Trois Fourches Tortonian basin, and a younger normal
 367 sense of movement imprinting Tortonian pyroclastic layer nearby El Addi (Fig. 3).

368 To the east, the coast of the peninsula corresponds to the Râs Izemrân Fault that
 369 strikes NNE-SSW and has high dips towards the ESE. This normal fault shows a normal
 370 regime with a small left-handed oblique component (Fig. 12C).

371 The Mersa Taïdant Fault (Figs 3, 4, and 12A) is a normal right-handed brittle fault,
 372 which extends from the Oued Amekrane to the coast line cutting across all the
 373 aforementioned faults (Fig. 3, 4, 12A). This fault has N110°E strike and dips to the
 374 southwest. On the western border of the massif, another normal fault (Oued Amekrâne
 375 Fault, OAF in Fig. 3) striking N155°E bounds the metamorphic basement from the
 376 Neogene sediment. This normal fault following the Oued Amekrâne is dipping 80° to the
 377 west.

378 We have measured several small faults along the trace of the Aït Lahsene, Râs
 379 Izemrân, and Oued Amekrâne faults (see Figs. 12D to I) that show both normal and reverse
 380 slip kinematics. The right-dihedral method (Angelier and Mechler, 1977) allows us
 381 reconstructing the palaeostress axes from fault populations. The σ_1 , σ_2 , and σ_3 axes are
 382 trending NNW-SSE, subvertical, and WSW-ENE, respectively. A late open-radius
 383 antiform exhibiting an E-W trending axes gently deforms the bedding of the Tortonian
 384 rocks together with the basement rock, and probably also the aforementioned faults.

385

386 **6.-Discussion**

387 The geochemistry of the orthogneisses shows that both major and trace elements
 388 have been mobilised during the main metamorphism event that agrees with the later

389 metasomatic event producing kaolinite in the metasediments (see Negro et al., 2007, 2008).
 390 However, the data document that the protoliths of the rocks were peraluminous granitoids,
 391 and specifically magnesian ones according to Frost et al. (2001) (Fig. 5).

392 In the silicate Earth-normalised diagrams, they have negative anomalies in Ba, Nb,
 393 Sr, Zr, and Ti; and positive anomalies in U, Ta, Pb, and P (Fig. 7), suggesting a crustal-
 394 derived signature. These rocks have low contents in REE, and also have chondrite-
 395 normalised enrichment in LREE relative to HREE with negative Eu anomalies (Fig. 7).
 396 The low values of $^{87}\text{Rb}/^{86}\text{Sr}$ (3.002 and 10.241) of the orthogneisses suggests that Rb has
 397 been mobilized in these rocks agreeing with the previously mentioned metasomatic event,
 398 while the $^{147}\text{Sm}/^{144}\text{Nd}$ (0.166 and 0.169), $\epsilon\text{Nd}_{335\text{Ma}}$ (-3.3 and -4.1) and $T_{\text{DM(Ga)}}$ (2.0 and 2.2)
 399 suggest a significant crustal component that agrees with the crustal-derived signature.

400 The obtained U-Pb SHRIMP on zircons ages range from 290 to 295 Ma suggesting
 401 a Sakmarian (Early Permian) age for the intrusion of the protoliths of the gneisses.
 402 Intrusive bodies at the origin of the protoliths are probably related to the Late Variscan
 403 magmatic event that is reported throughout the entire Variscan Belt (i.e. Bea, 2004;
 404 Casquet and Galindo, 2004; Pereira et al., 2012).

405 The early Permian age for the igneous protoliths also indicates that the
 406 metasedimentary sequence of the upper Tarjât Unit has a Carboniferous or older age. The
 407 age of the sequence of the lower Taïdant Unit cannot be determined in the Cap des Trois
 408 Fourches area. However, similarities with the early Cretaceous (Aptian-Albian) brown
 409 shales and quartzites of the intermediate Temsamane units, together with a similar location
 410 below a chloritoid-bearing Paleozoic IP-LT metamorphic unit (Ras Afrou Unit in the
 411 Temsamane mountain range and Tarjât unit in the Trois Fourches Peninsula, see Frizon de
 412 Lamotte, 1985; Frizon de Lamotte et al., 1991; Azdimousa et al., 2007; Negro et al., 2007,

413 2008; Jabaloy et al., 2015) suggest an early Cretaceous age for the green and brown shales
 414 of the lower Taïdant Unit.

415 The $^{40}\text{Ar}/^{39}\text{Ar}$ age analyses of muscovite porphyroclasts from the mylonites (AP3-F
 416 sample) are very difficult to interpret due to the disturbed spectra of all the replicates.
 417 However, it must be emphasized that the muscovite have retained an uppermost Triassic
 418 age at around 202 Ma and have not been re-equilibrated during the later metamorphic
 419 events (Negro et al., 2007, 2008; Jabaloy et al., 2015). This uppermost Triassic age from
 420 the sample AP3-F could be interpreted as a cooling age following the heat anomaly related
 421 to the rifting leading to the opening of the Tethys Ocean. Whatever is the possible origin of
 422 the heat event, the most likely interpretation is a partial re-opening of the system in relation
 423 with fluids circulation during the mylonitisation processes but at an undetermined age.

424 Similarities with the Temsamane fold-and-thrust stack include far more than the
 425 presence of the chloritoid-bearing Paleozoic IP-LT metamorphic unit. The meso and
 426 macrostructures described in this work correlate properly with those previously described
 427 in the Temsamane mountain range by Frizon de Lamotte (1985), Frizon de Lamotte et al.
 428 (1991), Azdimousa et al. (2007), Booth-Rea et al. (2012) and Jabaloy et al. (2015).

429 The planar-linear fabric (S_p/L_p) generated in a non-coaxial deformation with a top-
 430 to-the-WSW is present in both situations as the main mesostructures and the subsequent
 431 SE verging NE-SW trending major folds (F_c) deforming the fabric. Also, in good
 432 agreement are: (1) the IP-LT metamorphic conditions recognized in the uppermost
 433 metamorphic unit (Negro et al., 2007 and 2008), and (2) the $^{40}\text{Ar}/^{39}\text{Ar}$ ages indicating that
 434 the main metamorphic event took place during the Chattian–Aquitanian times (Negro et
 435 al., 2008; Jabaloy et al., 2015).

436 García-Dueñas et al. (1995) and Sánchez-Gómez (1996) have ascribed the rocks of
 437 the Tarjât Unit to the Sebtide/Alpujarride Complex from the Internal Zones of the

438 Rif/Betic belt. Because the Taïdant Unit is in the uppermost structural situation, they have
 439 proposed this unit to be part of the Ghomaride/Malaguide Complex of the Internal Zones.
 440 Michard et al. (2007, 2008) have provided the same tectonic interpretation for the Taïdant
 441 Unit being in the uppermost position. However, instead of proposing any relationship with
 442 the Rif/Betic Internal Zones they correlated the Taïdant Unit with the Ketama Unit and the
 443 Tarjât Unit to the highest most metamorphic Temsamane Unit (i.e. the External Zone of
 444 the Rif) (Michard et al., 2007, their Fig. 8).

445 The horizontal brittle-ductile fault at the base of the Taïdant Unit and outcropping
 446 at the sea level strongly resembles the fault rocks association, kinematics and geometry of
 447 the Temsamane detachment as described by Booth-Rea et al. (2012) and Jabaloy et al.
 448 (2015). More precisely, the Cap des Trois Fourches area is similar to the brittle Ait
 449 Amrâne klippen and the Khebaba semi-klippe where IP-LT metamorphic rocks are
 450 separated by brittle fault rocks from the lowermost Temsamane units (Booth-Rea et al.,
 451 2012; Jabaloy et al. 2015). The Tortonian and Messinian sediments and volcanic rocks
 452 covering the subhorizontal detachment fault indicate that this fault was exposed at eroding
 453 agents during Tortonian times. This is in good agreement with the evolution described in
 454 the Boudinar basin further west (Azdimousa et al., 2006; Galindo-Zaldivar et al., 2015;
 455 Jabaloy et al., 2015; Achalhi et al., 2016). The last brittle deformation events have
 456 recorded a NNW-SSE compression and a WSW-ENE extension of Messinian age. We
 457 therefore suggest that the Cap des Trois Fourches Paleozoic rocks are part of the
 458 Temsamane fold-and-thrust stack. This interpretation has been previously proposed by
 459 Michard et al. (2007, 2008). Also, it was considered that the Paleozoic rocks of the Cap des
 460 Trois Fourches extend eastwards into the Kebdana range and western Algeria. As a
 461 consequence, we consider that the Paleozoic sediments and igneous rocks of the Cap des
 462 Trois Fourches together with the along-trending similar units are remains derived from the

463 North African palaeomargin involved in the Rif belt. These units were involved as tectonic
 464 sheets in the External Zone of the Rif, and originated most probably from the Eastern
 465 Moroccan Meseta. They have first recorded the Triassic rifting events and then the
 466 collision between the Internal Zones of the Rif belt (i.e. the Alborán domain) and the
 467 Tethysian margin of the Africa plate during the Cenozoic times.

468 As previously mentioned in the geological setting section, the western and eastern
 469 Rif exhibit a major contrast in their structural level of tectonic deformation. This is in good
 470 agreement with the crustal thickness of both areas that are ~50 km to ~ 24 km,
 471 respectively (Mancilla et al., 2012, 2015; Díaz et al., 2016). We infer that the crustal
 472 transition step between both domains is located along the active Trougout-Nekor sinistral
 473 transtensional system (Asebriy et al., 1993; Barcos et al., 2014; Poujol et al., 2014) at
 474 subsurface shallower depth. This transtensional zone system that involves the lithosphere-
 475 asthenosphere boundary at depth is considered as accommodating the Present-day
 476 movement of the Western Rif towards the WSW with respect to the stable Nubia (see GPS
 477 data from Vernant et al., 2010). Thus, forming the southern STEP boundary of the Betic-
 478 Rif subduction system. Upward, the active Trougout-Nekor system would be the signature
 479 of the crustal step (Fig. 13, location of the cross-section on Fig. 2) at shallower depth. The
 480 ductile tectonic deformation identified at the Cap des Trois Fourches together with those
 481 recognized in the Temsamane area document a major detachment: the Temsamane
 482 detachment system, whose hanging wall moved towards the SW (Azdimousa et al., 2007;
 483 Booth-Rea et al., 2012; Jabaloy et al., 2015). To the west, the active Trougout-Nekor fault
 484 system (Asebriy et al., 1993; Barcos et al., 2014; Poujol et al., 2014) records a sinistral
 485 transtensional movement. This fault system cuts the Temsamane detachment, which is
 486 displaced downward by about several km bounding the Ketama unit at depth. At Present

487 time, this detachment is active bounding the western Rif at depth that is moving as a
 488 whole, being the hanging wall of the system.

489 The cross section at Figure 13 agrees with the roll-hinge model (Buck, 1988;
 490 Hamilton, 1988; and Wernicke and Axen, 1988; Lavier et al., 1999; Platt et al. 2014)
 491 where the Trougout-Nekor fault system is the active section of the detachment whose
 492 hanging wall is moving around 4 mm/year⁻¹ towards the WSW. The Temsamane
 493 detachment represents the inactive section of the detachment as previously proposed by
 494 Booth-Rea et al. (2012) and Jabaloy et al. (2015). The strong thinning of the crust along
 495 the eastern Rif, which occurred since the Late-Neogene is proposed resulting from the
 496 Temsamane detachment fault system at the southern edge of the Betic-Rif subduction
 497 system.

498

499

500 **7.-Conclusions**

501 We present new lithostratigraphic and geochemical data from the Cap des Trois
 502 Fourches area. We describe and date for the first time mylonitised orthogneisses derived
 503 from Late Variscan magnesian peraluminous granitoids. Their protoliths were
 504 subsequently involved into the Alpine orogeny and associated metamorphism. We also
 505 redefine the major metamorphic sequences from the area and we clarify their tectonic
 506 relationship. We present a new cartography of the area defining the extension of the
 507 Taïdant and Tarjât units and their internal tectonic deformations. A major ductile shear
 508 zone separates the Upper Tarjât unit from the Lower Taïdant unit. Tectonic deformation
 509 kinematics of the shear zone documents a top-to-the-west sense of movement.

510 Also, we have identified a major ductile-brittle detachment fault with a top-to-the-
 511 west sense of movement. We infer this detachment being an eastward prolongation of the

512 Temsamane detachment into the des Cap des Trois Fourches area. We provide new U-Pb
 513 SHRIMP zircon ages from the orthogneisses indicating a Sakmarian (Early Permian) age
 514 for the intrusion of their protoliths. We also determine $^{40}\text{Ar}/^{39}\text{Ar}$ ages in micro-populations
 515 (2 to 3 grains) of white micas from the mylonitised orthogneisses with a weighted mean
 516 age of 202.45 ± 0.98 Ma. That age is more probably related to a partial re-opening of the
 517 system in relation with fluids circulation during the mylonitisation processes, but at an
 518 undetermined age.

519 We propose a model of the crustal structure of the eastern Rif, where the brittle
 520 detachment represents the inactive section from an active detachment responsible for the
 521 Present-day movement of the central Rif with respect to the eastern Rif and the different
 522 crustal thicknesses between both sectors.

523

524 **Acknowledgements**

525 We acknowledge the financial support of research grants CGL2015-71692-P and
 526 CGL2015-67130-C2-1-R from the Spanish Ministry of Economy and Competitiveness
 527 (MINECO/FEDER, Spain). This project has received funds from the FP7-Marie Curie
 528 Action IRSES-MEDYNA funded under Grant Agreement PIRSES-GA- 2013-612572. We
 529 want to thank Aitor Cambeses for his help with the geochemistry and geochronology of the
 530 orthogneisses, and Fernando Nieto for his help with the adquisition and interpretation of
 531 the XRD data.

532

533 **References:**

534 Achalhi, M., Münch, P., Cornée,J.-J. , Azdimousa, A., Melinte-Dobrinescu, M.,
 535 Quillévéré, F., Drinia, H., Fauquette, S., Jiménez-Moreno, G., Merzeraud, G., Ben
 536 Moussa, A., El Kharim, Y., Feddi, N., 2016. The late Miocene Mediterranean-

- 537 Atlantic connections through the North Rifian Corridor: New insights from the
 538 Boudinar and Arbaa Taourirt basins (northeastern Rif, Morocco). *Palaeogeography,*
 539 *Palaeoclimatology, Palaeoecology*, 459, 131–152.
- 540 Ait Brahim, L., 1991. Tectonique cassante et états de contraintes récents au nord du Maroc;
 541 contribution à l'étude du risque sismotectonique. Ph. Doctoral Thesis, University of
 542 Rabat, Morocco, 360 p.
- 543 Amar, N., Khattach, K., Azdimousa, A., Chourak, M., Jabaloy, A., Ahmed Manar, A.,
 544 Amar, M., 2015. Structure and peridotite of Gibraltar arc southern bloc: gravimetric
 545 and aeromagnetic evidences. *Arab. J. Geosci.* 8, 11, 9801-9813. doi :
 546 10.1007/s12517-015-1879-3.
- 547 Angelier, J., Mechler, P., 1977. Sur une méthode graphique de recherche des contraintes
 548 principales également utilisable en tectonique et en séismologie: la méthode des
 549 dièdres droits. *Bull. Soc. Geol. Fr.* 7, 6, 1309-1318.
- 550 Andrieux, J., 1971. La structure du Rif central. Notes du Service Géologique du Maroc
 551 (235 pp., Rabat, Morocco).
- 552 Asebriy, L., 1994. Evolution tectonique et métamorphique du Rif central (Maroc):
 553 définition du domaine Subrifain. Ph. Doctoral Thesis,, University of Rabat,
 554 Morocco, 248 pp.
- 555 Asebriy, L., de Luca, P., Bourgois, J., Chotin, P., 1987. Resédimentation d'âge sénonien
 556 dans le Rif central (Maroc): conséquences sur les divisions paléogeographiques et
 557 structurales de la chaîne. *J. Afr. Earth Sci.* 6, 9–17.
- 558 Asebriy, L., Bourgois, J., Cherkaoui, T.E., Azdimousa, A., 1993. Evolution tectonique
 559 récente de la zone de faille du Nékor: importance paléogeographique et structurale
 560 dans le Rif externe, Maroc. *J. African Earth Sci.*, 17, 65–74.

- 561 Asebriy, L., Azdimousa, A., Bourgois, J., 2003. Structure du Rif externe sur la transversale
 562 du Massif de Ketama. *Trav. Inst. Sci. Rabat, Maroc* 21, 27–46.
- 563 Azdimousa, A., Bourgois, J., Poupeau, G., Montigny, R., 1998. Histoire thermique du
 564 massif de Kétama (Maroc); sa place en Afrique du Nord et dans les Cordillères
 565 Bétiques. *C. R. Acad. Sci. Paris* 326, 847–853.
- 566 Azdimousa, A., Bourgois, J., Asebriy, L., Poupeau, G., Montigny, R., 2003. Histoire
 567 thermique et surrection du Rif externe et des nappes de flyschs associées (Nord
 568 Maroc). *Trav. Inst. Sci. Rabat*, 21, 15–26.
- 569 Azdimousa, A., Poupeau, G., Rezqui, H., Asebriy, L., Bourgois, J., Aït Brahim, L., 2006.
 570 Géodynamique des bordures méridionales de la mer d'Alboran; application de la
 571 stratigraphie séquentielle dans le bassin néogène de Boudinar (Rif oriental, Maroc).
 572 *Bull. Inst. Sci. Rabat Sci. Terre*, 28, 9–18.
- 573 Azdimousa, A., Jabaloy, A., Asebriy, L., Booth-Rea, G., González-Lodeiro, F., Bourgois,
 574 J., 2007. Lithostratigraphy and structure of the Temsamane unit (eastern external
 575 Rif, Morocco). *Rev. Soc. Geol. Esp.* 20, 187–200.
- 576 Balanyá, J.C., García-Dueñas, V., 1987. Les directions structurales dans le Domaine
 577 d'Alborán de part et d'autre du Détriot de Gibraltar. *C. R. Acad. Sci.*, 304, 929–932.
- 578 Barcos, L., Jabaloy, A., Azdimousa, A., Asebriy, L., Gómez-Ortiz, D., Rodríguez-Peces,
 579 M.J., Tejero, R., Pérez-Peña, J.V., 2014. Study of relief changes related to active
 580 doming in the eastern Moroccan Rif (Morocco) using geomorphological indices.
 581 *J. Afr. Earth Sci.*, 100, 493–509.
- 582 Bea, F., 2004. La naturaleza del magmatismo de la Zona Centro Ibérica: consideraciones
 583 generales y ensayo de correlación. In: Vera, J. A. (Ed.), *Geología de España*. 128–
 584 133. Madrid: SGE-IGME.

- 585 Ben Yaich, A., 1991. Evolution tectono sédimentaire du Rif externe centro occidental
 586 (Régions de Msila et Ouezzane, Maroc). La marge africaine du Jurassique au
 587 Crétacé inférieur. Les bassins néogènes d'avant fosse. PhD Thesis, University of
 588 Pau, France, 308 p
- 589 Benzaggagh, M., Mokhtari, A., Rossi, P., Michard, A., El Maz, A., Chalouan, A., Saddiqi,
 590 O., Rjimati, E.-C., 2014. Oceanic units in the core of the External Rif (Morocco):
 591 intramargin hiatus or South-Tethyan remnants? *J. Geodyn.* 77, 4–21. doi:
 592 10.1016/j.jog.2013.10.003.
- 593 Bezada, M.J., Humphreys, E.D. Toomey, D.R., Harnafi, M., Davila, J.M., 2013. Evidence
 594 for slab rollback in westernmost Mediterranean from improved upper mantle
 595 imaging, *Earth Planet. Sci. Lett.* 368, 51-60.
- 596 Booth-Rea, G., Azañón, J.M., Martínez-Martínez, J.M., Vidal, O., García-Dueñas, V.,
 597 2005. Contrasting structural and P–T evolutions of tectonic units in the southeastern
 598 Betics: key for understanding the exhumation of the Alborán Domain HP/LT
 599 crustal rocks (Western Mediterranean). *Tectonics* 24. doi: 10.1029/2004TC001640.
- 600 Booth-Rea, G., Ranero, C.R. Martínez-Martínez, J.M. Grevemeyer, I., 2007. Crustal types
 601 and Tertiary tectonic evolution of the Alborán Sea, western Mediterranean.
 602 *Geochemistry, Geophysics, Geosystems* 8 (10), Q10005.
- 603 Booth-Rea, G., Jabaloy-Sánchez, A., Azdimousa, A., Asebriy, L., Vázquez-Válchez, M.,
 604 Martínez-Martínez, J.M., 2012. Upper-crustal extension during oblique collision:
 605 the Temsamane extensional detachment (eastern Rif, Morocco). *Terra Nova* 24,
 606 505–512. doi: 10.1111/j.1365-3121.2012.01089.x.
- 607 Booth-Rea, G., Ranero, C.R., Grevemeyer, I., in press. The Alboran volcanic arc modulated the
 608 Messinian faunal exchange and salinity crisis. *Scientific Reports* in press. Doi:10.1038/s41598-
 609 018-31307-7.

- 610 Bourgois, J., 1977. D'une étape géodynamique majeure dans la genèse de l'arc de
 611 Gibraltar: L'hispanisation des flyschs rifains au Miocène inférieur. Bull. Soc. Geol.
 612 Fr. XIX, 115–1119.
- 613 Bourgois, J., 1980a. Pre-Triassic fit and alpine tectonics of continental blocks in the western
 614 Mediterranean: discussion and reply. Geological Society of America Bulletin, 91,
 615 632-634.
- 616 Bourgois, J., 1980b. De l'origine ultra-bétique des Malaguides (zones internes bétiques,
 617 Espagne). Geologica Romana, 19, 151-170.
- 618 Buck, W. R., 1988. Flexural rotation of normal faults, Tectonics, 7, 959 – 973.
- 619 Calvert, A., Sandvol, E., Seber, D., Barazangi, M., Roecker, S., Mourabit, T., Vidal, F.,
 620 Alguacil, G., Jabour, N., 2000 Geodynamic evolution of the lithosphere and upper
 621 mantle beneath the Alboran region of the western Mediterranean: constraints from
 622 travel time tomography. J Geophys Res 105, 10871-10898.
- 623 Carminati, E., Lustrino, M., Doglioni, C., 2012. Geodynamic evolution of the central and
 624 western Mediterranean::Tectonics vs. igneous petrology constraints.
 625 Tectonophysics 579, 173-192
- 626 Casquet, C., Galindo, C., 2004. El magmatismo varisco de la Zona de Ossa
 627 Morena. In: Geología de España. Vera, J.A. (ed.) SGE-IGME, Madrid, 194-
 628 199, ISBN: 84-7840-546-1.
- 629 Chalouan, A., Michard, A., 2004. The Alpine Rif belt (Morocco): a case of mountain
 630 building in a subduction-subduction-transform fault triple junction. Pure Appl.
 631 Geophys. 161 (3), 489–519.
- 632 Chalouan, A., Michard, A., El Kadiri, K., Negro, F., Frizon de Lamotte, D., Soto, J.I.,
 633 Saddiqi, O., 2008. The Rif Belt. In: Michard, A., Frizon de Lamotte, D., Saddiqi,
 634 O., Chalouan, A. (Eds.), Continental Evolution: The Geology of Morocco, Lecture

- 635 Notes in Earth Sciences. vol. 116. Springer-Verlag, Berlin Heidelberg, pp. 203–
 636 302.
- 637 Chertova, M.V., Spakman, W., van den Berg, A.P., van Hinsbergen, D.J.J., 2014. Absolute
 638 plate motions and regional subduction evolution. *Geochemistry, Geophysics,
 639 Geosystems* 15, 3780-3792, doi: 10.1002/2014GC005494.
- 640 Díaz, J., Gil, A., Carbonell, R., Gallart J., Harnafī, M., 2016. Constraining the crustal root
 641 geometry beneath Northern Morocco, *Tectonophysics*. 689, 14-24. doi:
 642 10.1016/j.tecto.2015.12.009.
- 643 Duggen, S., Hoernle, K., van den Bogaard, P., Rupke, L., Phipps Morgan, J., 2003. Deep roots of the
 644 Messinian salinity crisis. *Nature* 422, 602-606.
- 645 Duggen, S., Hoernle, K., Van den Bogaard, P., Garbe-Schonberg, D., 2005. Post-
 646 collisional transition from subduction- to intraplate-type magmatism in the
 647 Westernmost Mediterranean: evidence for continental-edge delamination of
 648 subcontinental lithosphere. *J. Petrol.* 46, 1155–1201.
- 649 Duggen, S., Hoernle, K., Klugel, A., Geldmacher, J., Thirlwall, M., Hauff, F., Lowry, D., Oates, N.,
 650 2008. Geochemical zonation of the Miocene Alboran Basin volcanism (westernmost
 651 Mediterranean): geodynamic implications. *Contrib Mineral Petr* 156, 577-593.
- 652 Durand-Delga, M., Hottinger, L., Marcais, J., Mattauer, M., Milliard, Y., Suter, G., 1962.
 653 Données actuelles sur la structure du Rif. Livre à la mémoire du professeur Fallot.
 654 Soc. Géol. Fr. Mém. 1, 399–442 (Paris).
- 655 Duran-Delga, M., Rossi, P., Olivier, P., Puglisi, D., 2000. Situation structurale et nature
 656 ophiolitique de roches basiques jurassiques associées aux flyschs maghrébins du
 657 Rif (Maroc) et de Sicile (Italie). *C. R. Acad. Sci. Paris II* 331 (1), 29–38.

- 658 Faccenna, C., Piromallo, C., Crespo-Blanc, A., Jolivet, L., Rossetti, F., 2004. Lateral slab
 659 deformation and the origin of the western Mediterranean arcs. *Tectonics* 23. doi:
 660 10.1029/2002TC001488.
- 661 Favre, P., 1992. Géologie des massifs calcaires situés au front Sud de l'unité de Kétama
 662 (Rif, Maroc). PhD Thesis. University of Genève.
- 663 Feinberg, H., 1986. Les séries tertiaires du Pré rif et des dépendances post tectoniques du
 664 Rif (Maroc). PhD Thesis, University of Toulouse.
- 665 Fernandez Navarro, L., 1911. Estudios geológicos del Rif oriental. *Memorias de Real
 666 Sociedad Española de Historia Natural*. Tome XIII
- 667 Frizon de Lamotte, D., 1985. La structure du Rif oriental (Maroc). Rôle de la tectonique
 668 longitudinale et importance des fluides. Ph.D. Thesis, University Paul et Marie
 669 Curie, Paris VI, France (436 pp.).
- 670 Frizon de Lamotte, D., 1987. Un exemple de collage synmétamorphe: la déformation
 671 miocène des Temsamane (Rif externe, Maroc). *Bull. Soc. Geol. Fr.* 3, 337–344.
- 672 Frizon de Lamotte, D., Andrieux, J., Guezou, J.-C., 1991. Cinématique des
 673 chevauchements néogènes dans l'Arc bético-rifain: discussion sur les modèles
 674 géodynamiques, *Bull. Soc. Géol. Fr.*, 169, 611-626.
- 675 Frost, B.R., Arculus, R.J., Barnes, C.G., Collins, W.J., Ellis, D.J., Frost, C.D., 2001. A
 676 geochemical classification of granitic rocks. *Journal of Petrology*, 42, 2033-2048.
- 677 Galindo-Zaldívar, J., Azzouz, O., Chalouan, A., Pedrera, A., Ruano, P., Ruiz-Constán, A.,
 678 Sanz de Galdeano, C., Carlos Marín-Lechado, C., López-Garrido, A-C., Anahnah,
 679 A., Benmakhlouf, M., 2015. Extensional tectonics, graben development and fault
 680 terminations in the eastern Rif (Bokoya– Ras Afraou area). *Tectonophysics*, 663,
 681 140- 149. doi: 10.1016/j.tecto.2015.08.029

- 682 García-Dueñas, V., Balanyá, J.C., Sánchez-Gómez, M., 1995. El Despegue extensional de
683 Lahnene y los jirones de serpentinitas del anticlinal de Taryat (Melilla, Rif).
684 Geogaceta, 17, 138–139.
- 685 Govers, R., Wortel, M.J.R., 2005. Lithosphere tearing at STEP faults: response to edges of
686 subduction zones. Earth Planet Sc Lett 236, 505-523.
- 687 Guillemin, M., Hernandez, J., Wildi, W., 1983. Carte géologique du Rif, échelle 1/50 000,
688 feuille Melilla. Notes et Mémoires du Service géologique du Maroc, 297.
- 689 Guillemin, M., Houzay, J. P., 1982. Le Néogène post-nappes et le Quaternaire du Rif Nord
690 oriental. Stratigraphie et tectonique des bassins de Melilla, de Kert, de Boudinar et
691 du piémont des Kebdana. Notes et Mémoires du Service Géologique du Maroc,
692 314, 7–239.
- 693 Hamilton, W.B., 1988. Detachment faulting in the Death Valley region, California and
694 Nevada: U.S. Geological Survey Bulletin, 1790, 51–85.
- 695 Hermann, J., Müntener, O., Scambelluri, M., 2000. The importance of serpentinite
696 mylonites for subduction and exhumation of oceanic crust. Tectonophysics, 327,
697 225-238.
- 698 Hernández, J., Bellón, H., 1985. Chronologie K-Ar du volcanisme miocène du Rif oriental
699 (Maroc): implications tectoniques et magmatologiques. Revue de Géologie
700 Dynamique et de Géographie Physique, 26, 85-94.
- 701 Jabaloy-Sanchez, A., Azdimousa, A., Booth-Rea, G., Asebriy, L., Vazquez-Vilchez, M.,
702 Miguel Martinez-Martinez, J., Gabites, J., 2015. The structure of the Temsamane
703 fold-and-thrust stack (eastern Rif, Morocco): Evolution of a transpressional
704 orogenic wedge. Tectonophysics, 663, 150-176. Doi: 10.1016/j.tecto.2015.02.003.

- 705 Jolivet, L., Faccenna, C., Goffé, B., Burov, E., Agard, P., 2003. Subduction tectonics and
 706 exhumation of high-pressuremetamorphic rocks in the Mediterranean orogens. Am.
 707 J. Sci., 303, 353–409.
- 708 Kerzazi K., 1994. Etudes biostratigraphique du Miocène sur la base des foraminifères
 709 planctoniques et nannofossiles calcaires dans le Pré rif et la marge atlantique du
 710 Maroc (site 547A du DSDP Leg 79); aperçu sur leur paléoenvironnement. PhD
 711 Thesis, University Pierre et Marie Curie, Paris, 230 pp.
- 712 Lavier, L.L., Buck, W.R., Poliakov, A.N.B., 1999, Self-consistent rolling-
 713 hinge model for the evolution of large-offset low-angle normal faults:
 714 Geology, 27, 1127–1130.
- 715 Leblanc, D., 1975–1979. Etude géologique du Rif externe oriental au Nord de Taza
 716 (Maroc). Notes et Mémoires du Service Géologique du Maroc, 281 p.
- 717 Le Maitre, R.W., 1989. A Classification of Igneous Rocks and Glossary of Terms.
 718 Recommendations of the IUGS Commission on the Systematics of Igneous Rocks.
 719 Oxford, Blackwell, 256 pp.
- 720 Levy, R.G., Tilloy, R., 1952. Maroc septentrional (chaîne du Rif). Partie B, livret guide des
 721 excursions A31.C31. In : Congrès Géologique International, XIX session- Alger,
 722 série : Maroc, pp 8-65.
- 723 Mancilla, F. L., Stich, D., Morales, J., Julià, J., Diaz, J., Pazos, A., Córdoba, D., Pulgar,
 724 J.A., Ibarra, P., Harnafi, M., Gonzalez-Lodeiro, F., 2012. Crustal thickness
 725 variations in northern Morocco. J. Geophys. Res., 117, B02312. doi:
 726 10.1029/2011JB008608.
- 727 Mancilla, F.L., Booth-Rea, G., Stich, D., Pérez-Peña, J. V., Moreles, J., Azañón, J. M.,
 728 Martin, R., Flavio Giaconia, F., 2015. Slab rupture and delamination under the

- 729 Betics and Rif constrained from receiver functions. *Tectonophysics*, 663, 225–237.
- 730 doi : 10.1016/j.tecto.2015.06.028
- 731 Mancilla, F.L., Diaz, J., 2015. High resolution Moho topography map beneath Iberia and
- 732 Northern Morocco from receiver function analysis. *Tectonophysics*, 203–211, doi:
- 733 10.1016/j.tecto.2015.06.017.
- 734 Martínez-Martínez, J.M., Booth-Rea, G., Azañón, J.M., Torcal, F., 2006. Active transfer
- 735 fault zone linking a segmented extensional system (Betics, southern Spain): Insight
- 736 into heterogeneous extension driven by edge delamination. *Tectonophysics* 422,
- 737 159–173.
- 738 McDonough, W.F., Sun, S.S., 1995. The composition of the Earth. *Chemical Geology*,
- 739 120, 223–253.
- 740 Michard, A., 1976. Elements de Géologie Marocaine. Notes Mémoires du Service
- 741 Géologique du Maroc 258, 408.
- 742 Michard, A., Feinberg, H., El-Azzab, D., Bouybaouène, M., Saddiqi, O., 1992. A
- 743 Serpentinite ridge in a collisional paleomargin setting: the Beni Malek Massif,
- 744 external Rif, Morocco. *Earth Planet. Sci. Lett.* 113 (3), 425–442.
- 745 Michard, A., Frizon de Lamotte, D., Negro, F., Saddiqi, O., 2007. Serpentinite slivers and
- 746 metamorphism in the External Maghrebides: arguments for an intracontinental
- 747 suture in the African paleomargin (Morocco, Algeria). *Rev. Soc. Geol. Esp.* 20,
- 748 173–185.
- 749 Michard, A., Hoepffner, A., Soulaimana, A., Baider, L., 2008. The Variscan Belt. In
- 750 Michard, A.; Saddiqi, O.; Chalouan, A.; Frizon de Lamotte, D., eds. *Continental*
- 751 *evolution: the geology of Morocco*. Berlin, Springer, 133–202.
- 752 Monié, P., Frizon de Lamotte, D., Leikine, M., 1984. Etude géochronologique préliminaire
- 753 par la méthode $^{39}\text{Ar}/^{40}\text{Ar}$ du métamorphisme alpin dans le Rif externe (Maroc).

- 754 Précisions sur le calendrier tectonique tertiaire. Revue du Géologie Dynamique et
 755 du Géographie physique, 25, 307-317.
- 756 Morel, J.L. (1988) Evolution récente de l'orogène rifain et de son avant-pays depuis la fin
 757 de la mise en place des nappes (Rif, Maroc). Geodiffusion Mémoires, University
 758 Paris-Sud, 4, 583 pp.
- 759 Münch, P., Roger, S., Cornee, J.-J., Saint Martin, J.-P., Feraud, G., Benmoussa, A., 2001.
 760 Restriction des communications entre l'Atlantique et la Méditerranée au Messinien :
 761 apport de la téphrochronologie dans la plate-forme carbonatée et le bassin de
 762 Melilla–Nador (Rif nord-oriental, Maroc). C. R. Acad. Sci. 332, 9, 569–576.
- 763 Münch, P., Cornee, J.-J., Feraud, G., Saint Martin, J.-P., Ferrandini, M., Garcia, F.,
 764 Conesa, G., Moullade, M., Roger, S., 2006. Precise $^{40}\text{Ar}/^{39}\text{Ar}$ chronostratigraphy of
 765 the upper Messinian Melilla carbonate complex (NE Morocco): implications for the
 766 Messinian Salinity Crisis. International Journal of Earth Sciences, 95, 491–503.
- 767 Negro, F., 2005. Exhumation des roches métamorphiques du domaine d'Alboran: étude de
 768 la Chaîne Rifaine (Maroc) et corrélation avec les Cordillères Bétiques (Espagne).
 769 Ph.D. Thesis, University of Paris XI.
- 770 Negro, F., Agard, P., Goffé, B., Saddiqi, O., 2007. Tectonic andmetamorphic evolution of
 771 the Temsamane units, External Rif (northern Morocco): implications for the
 772 evolution of the Rif and the Betic–Rif arc. J. Geol. Soc. Lond. 164, 829–842.
- 773 Negro, F., de Sigoyer, J., Goffé, B., Saddiqi, O., Villa, I.M., 2008. Tectonic evolution of
 774 the Betic–Rif arc: new constraints from $^{40}\text{Ar}/^{39}\text{Ar}$ dating on white micas in the
 775 Temsamane units (External Rif, northern Morocco). Lithos, 106, 93–108. doi :
 776 10.1016/j.lithos.2008.06.011.
- 777 Palomeras, I., Thurner, S., Levander, A., Liu, K., Villaseñor, A., Carbonell, R., Harnafi,
 778 M., 2014. Finite-frequency Rayleigh wave tomography of the western

- 779 Mediterranean: Mapping its lithospheric structure. Geochemistry, Geophysics,
 780 Geosystems 15, 140-160, doi:10.1002/2013GC004861.
- 781 Pereira, M.F., Chichorro, M., Silva, J.B., Ordóñez-Casado, B., Lee, J.K.W., Williams, I.S.,
 782 2012. Early Carboniferous wrenching, exhumation of high-grade metamorphic
 783 rocks and basin instability in SW Iberia: constraints derived from structural geology
 784 and U–Pb and 40Ar–39Ar geochronology. Tectonophysics, 558–559, 28–44.
- 785 Pereira, M.F., Solá, A. R., Chichorro, M., Lopes, L., Gerdes, A., Silva, J.B., 2012. North-
 786 Gondwana assembly, break-up and paleogeography: U-Pb isotope evidence from
 787 detrital and igneous zircons of Ediacaran and Cambrian rocks of SW Iberia.
 788 Gondwana Res., 22, 866–881.
- 789 Pérouse, E., Vernant, P., Chery, J., Reilinger, R., McClusky, S., 2010. Active surface
 790 deformation and sublithospheric processes in the western Mediterranean
 791 constrained by numerical models. Geology 38(9), 823-826, doi:10.1130/G30963.1.
- 792 Platt, J.P., Soto, J.I., Whitehouse, M.J., Hurford, A.J., Kelley, S.P., 1998. Thermal
 793 evolution, rate of exhumation, and tectonic significance of metamorphic rocks from
 794 the floor of the Alboran extensional basin, western Mediterranean. Tectonics 17,
 795 671-689.
- 796 Platt, J.P., Behr, W.M., Johansen, K., Williams, J.R., 2013. The Betic–Rif arc and its
 797 orogenic hinterland: a review. Ann. Rev. Earth Planet. Sci., 41, 14.1–14.45. doi: 10.
 798 1146/annurev-earth-050212-123951.
- 799 Platt, J. D., Rudnicki, J.W. Rice, J. R., 2014. Stability and localization of rapid shear in
 800 fluid-saturated fault gouge: 2. Localized zone width and strength evolution, J.
 801 Geophys. Res. Solid Earth, 119, 4334–4359, doi: 10.1002/2013JB010711.
- 802 Poujol, A., Ritz, J.-F., Tahayt, A., Vernant, P., Condomines, M., Blard, P.-H., Billant, J.,
 803 Vacher, L., Tibari, B., Hni, L., Koulali, A., 2014. Active tectonics of the Northern

- 804 Rif (Morocco) from Geomorphic and Geochronological Data. *J.Geodyn.*, 77, 70–
805 88.
- 806 Roger, S., Münch, P., Cornée, J.J., Saint Martin, J.P., Féraud, G., Pestrea, S., Conesa, A.,
807 Benmoussa, A., 2000. $^{40}\text{Ar}/^{39}\text{Ar}$ dating of the pre-evaporitic Messinian marine
808 sequences of the Melilla basin (Morocco): a proposal for some biosedimentary
809 events as isochrons around the Alboran Sea. *Earth and Planetary Science Letters*,
810 179, 101-113.
- 811 Rosenbaum, G., Lister, G.S., Duboz, C., 2002. Reconstruction of the tectonic evolution of
812 the western Mediterranean since the Oligocene. *J. Virtual Explor.* 8, 107-130.
- 813 Sánchez-Gómez, M., 1996. Emplazamiento intracortical y desmembramiento extensional
814 de los cuerpos peridotíticos de Ronda y del Rif (Arco de Gibraltar). Ph.D. Thesis,
815 University of Granada. Spain.
- 816 Seber, D., Barazangi, M., Ibenbrahim, A., Demnati, A., 1996. Geophysical evidence for
817 lithospheric delamination beneath the Alboran Sea and Rif-Betic mountains. *Nature*
818 379, 785-790.
- 819 Shand, S.J., 1947. *Eruptive Rocks. Their Genesis, Composition, Classification, and Their*
820 *Relation to Ore-Deposits with a Chapter on Meteorite.* New York, John Wiley &
821 Sons, 360 pp.
- 822 Suter, G., 1980a. Carte géologique du Rif, 1/500.000, Map 245a, Geol. Surv. of Morocco,
823 Rabat.
- 824 Suter, G., 1980b. Carte structurale du Rif, 1/500.000, Map 245b, Geol. Surv. of Morocco,
825 Rabat.
- 826 Thurner, S., Palomeras, I., Levander, A., Carbonell, R., 2014. Evidence for Ongoing
827 Lithospheric Removal in the Western Mediterranean: Ps Receiver Functions

- 828 Results From the PICASSO Project. *Geochemistry, Geophysics, Geosystems* 15,
 829 1113-1127, doi:10.1002/2013GC005124.
- 830 van Assen, E., Kuiper, K.F., Barhoun, N., Krijgsman, W., Sierro, F.J., 2006, Messinian
 831 astro chronology of the Melilla Basin: Stepwise restriction of the Mediterranean-
 832 Atlantic connection through Morocco: *Palaeogeography, Palaeoclimatology,*
 833 *Palaeoecology*, 238,15–31, doi: 10.1016/j.palaeo.2006.03.014.
- 834 Varas-Reus, M.I., Garrido, C.J., Marchesi, C., Bosch, D., Acosta-Vigil, A., Hidas, K.,
 835 Barich, A., Booth-Rea, G., 2017. Sr-Nd-Pb isotopic systematics of crustal rocks
 836 from the western Betics (S. Spain): Implications for crustal recycling in the
 837 lithospheric mantle beneath the westernmost Mediterranean. *Lithos*, 276, 45-61.
- 838 Vázquez, M., Asebriy, L., Azdimousa, A., Jabaloy, A., Booth-Rea, G., Barbero, L.,
 839 Mellini, M., González-Lodeiro, F., 2013. Evidence of
 840 extensionalmetamorphismassociated to Cretaceous rifting of the North-Maghrebian
 841 passive margin: the Tanger–Ketama unit (External Rif, northern Morocco). *Geol.*
 842 *Acta* 11, 277–293.
- 843 Vernant, P., Fadil, A., Mourabit, T., Ouazar, D., Koulali, A., Davila, J. M., Garate, J., Mc
 844 Clusky,S., . Reilinger, R. E., 2010. Geodetic constraints on active tectonics of the
 845 Western Mediterranean: Implications for the kinematics and dynamics of the
 846 Nubia-Eurasia plate boundary zone, *J. Geodyn.*, 49, 123–129,
 847 doi:10.1016/j.jog.2009.10.007.
- 848 Vidal, J.F., 1971. Une interprétation nouvelle des nappes du Pré rif central (Maroc) et ses
 849 conséquences sur la structure de leur substratum autochtone. *C. R. Acad. Sci.*,
 850 Paris, D 272, 24–27.
- 851 Villaseñor, A., Chevrot, S., Harnafi, M., Gallart, J., Pazos, A., Serrano, I., Córdoba, D.,
 852 Pulgar, J.A., Ibarra, P., 2015. Subduction and volcanism in the Iberia–North Africa

- 853 collision zone from tomographic images of the upper mantle. Tectonophysics 663,
 854 238-249.
- 855 Wernicke, B. and Axen, G.J., 1988. On the role of isostasy in the evolution of normal fault
 856 systems, Geology 16, 848-851.
- 857
- 858 **Figure captions:**
- 859
- 860 **Figure 1.-** Geological map of the northwestern Africa, including the velocity data of the GPS sites with
 861 respect to stable Nubia (Vernant et al., 2010). The location of the study area (Fig.2) is shown.
- 862
- 863 **Figure 2.-** A) Main geological domains of the Betic-Rif orogenic system surrounding the Alborán Sea.
 864 B) Geological map of the Eastern Rif area with the kinematic vectors from the ductile shear zones and
 865 the brittle faults (modified from Jabaloy et al., 2015). Velocity data of the GPS sites with respect to
 866 stable Nubia in red (Vernant et al., 2010). Location of Fig. 3 is shown. 1-1' shows the location of the
 867 Fig. 13 profile.
- 868
- 869 **Figure 3.-** Geological map of the Cap des Trois Fourches area. See Figure 2 for location. Red stars
 870 show the location of the orthogneisses samples. Yellow star marks the location of the chlorite sample.
 871 Main brittle faults: ALF–Aït Lahsene Fault, DBDF-Ductile-Brittle Detachment fault, MTF–Mersa
 872 Taïdant Fault, OAF–Oued Amekrâne Fault, RIF– Râs Izemrân Fault,. Location of Fig.4 cross-sections
 873 is shown.
- 874
- 875 **Figure 4.-** Geological cross-sections of the Cap des Trois Fourches area. See Fig. 3 for location. Key
 876 of Color is same as on Fig. 3.
- 877

878 **Figure 5.-**

879 A) Panoramic view (looking to the west) of the orthogneisses lens-shaped bodies within the
 880 grey chloritoid-bearing micaschists (the white bed at the upper left is 20 to 25 cm thick). B)
 881 Hand specimen of the orthogneis sample C3F, note the abundance of K feldspar
 882 porphyroblasts with σ -structures. See Fig. 3 for sample location. C to F) Orthogneisses whole-
 883 rock compositions: C) Total alkalis vs SiO₂ (TAS) (fields from Le Maitre, 1989). D) Molar
 884 Al₂O₃/(Na₂O+K₂O) vs Molar Al₂O₃/(CaO+ Na₂O+K₂O) (fields from Shand, 1947). E) Modified
 885 alkali-lime index diagram MALI = Na₂O + K₂O - CaO vs SiO₂ (Frost et al., 2001). F) Molar
 886 (FeOT +MgO)/(MgO) vs SiO₂ (Frost et al. 2001). Th–Tholeiitic; Ca–Calc-alkaline; Alk–
 887 Alkaline.

888

889 **Figure 6.-** X-ray powder diffractogram of the chlorite sample CTF2. See Figure 3 for location.

890

891 **Figure 7.-** Silicate Earth- and chondrite-normalized diagrams of the orthogneisses (normalization
 892 values from McDonough and Sun (1995).

893

894 **Figure 8.-** A) Cathodoluminescence images of representative analyzed zircons of sample AP3-F. See
 895 Figure 3 for location. B) Wetherill concordia plot for the whole analyzed zircons from the sample AP3-
 896 F. C) Wetherill concordia plot for the analyzed zircons from the sample AP3-F with a higher age and
 897 more concordance. D) Cathodoluminescence images of representative analyzed zircons of sample C3F.
 898 See Figure 3 for location. E) Wetherill concordia plot for the whole analyzed zircons from the sample
 899 C3F. F) View of white mica mylonitized porphyroclasts from the sample AP3-F, similar to those used
 900 in ⁴⁰Ar/³⁹Ar determinations.

901

902 **Figure 9.-** Diagrams of cumulative ³⁹Ar Percent v. Age (Ma) of white mica mylonitized porphyroclasts

903 from the sample AP3-F. To the left, the replica with a mini-plateau age corresponding to 47% of ^{39}Ar ,
 904 of 205.49 ± 1.49 Ma, concordant with the total fusion age (205.88 ± 1.52 Ma). To the right, the three
 905 replicas without plateau ages (see text for discussion). In every graphic, the box heights are 2σ .

906

907 **Figure 10.-** Mesostructures from the Tarjât unit: A) upper view of the S_p foliation and L_p stretching
 908 lineation within grey chloritoid-bearing micaschists. B) Ductile S-C structure in the grey micaschists.
 909 C) Incipient S_c crenulation cleavage deforming the grey micaschists. D) mylonitic yellow marbles
 910 exhibiting asymmetric boudins of dolomitic marbles. E) View of the ductile shear zone duplicating the
 911 Tarjât unit, east of Oued Amekrâne. F and G) Diagrams representing the orientation of ductile
 912 mesostructures: F: L_p stretching lineation, and G) F_p axes of microfolds. For all the diagrams: Wulff
 913 steronet, lower hemisphere.

914

915 **Figure 11.-** Mesostructures from the Taïdant unit: A) view of the main foliation of the green and
 916 brown shales deformed by microfolds, and B) Diagram representing the orientation of the intersection
 917 lineation and microfold axis deforming the main foliation of the shales. For the diagram: Wulff
 918 steronet, lower hemisphere.

919

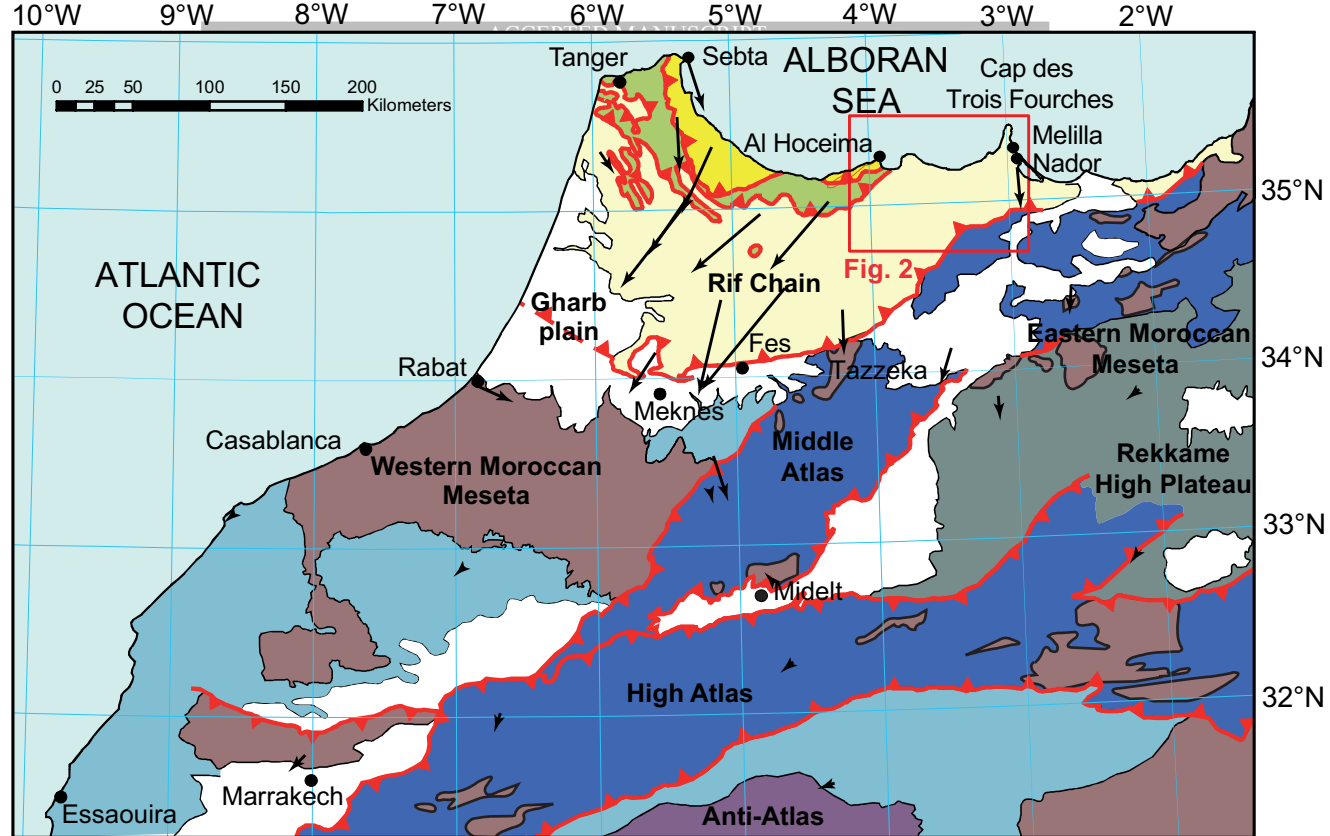
920 **Figure 12.-** A and B) View of the horizontal brittle-ductile fault and fault gouges outcropping at the
 921 coast that superposes out-of-sequence the Taïdant unit over the Tarjât one. C) View of the Râs
 922 Izemrân Fault zone. D and E) Diagram with the orientation of small faults along the trace of the Aït
 923 Lahsene Fault (D) and the result of the right-dihedral method (Angelier and Mechler, 1977) of the
 924 same fault population (E). F and G) Diagram with the orientation of small faults along the trace of the
 925 Râs Izemrân Fault (F) and the result of the right-dihedral method (Angelier and Mechler, 1977) of the
 926 same fault population (G). H and I) Diagram with the orientation of small faults along the trace of the
 927 Oued Amekrâne Fault (H) and the result of the right-dihedral method (Angelier and Mechler, 1977) of

928 the same fault population (I). For all the diagrams: Wulff steronet, lower hemisphere.

929

930 **Figure 13.-** A) Crustal model of the eastern Rif and the transition towards the central Rif area. The
931 Moho depths are from Mancilla et al. (2012, 2015) and Díaz et al. (2015), while the velocity data of the
932 GPS sites with respect to Nubia stable are from Vernant et al. (2010). B) Possible crustal model of the
933 eastern Rif before the movement of the Temsamane detachment fault during Late Miocene to Present-
934 day times.

935



- [White box] Neogene to Quaternary sedimentary basins
- [Light yellow box] External Rif
- [Light green box] Maghrebian Flyschs
- [Yellow box] Internal Rif
- [Dark blue box] Post-Hercynian cover deformed during the Alpine Orogeny
- [Light blue box] Post-Hercynian cover undeformed during the Alpine Orogeny
- [Grey box] Paleozoic Variscan Basement (Eastern Moroccan Meseta) and undeformed Post-Hercynian cover (Rekkame high plateau)
- [Purple box] Variscan foreland and Pan-African belt
- [Brown box] Caledonian-Variscan belt
- [Red arrow] Alpine major thrust and deformational front
- [Black arrow] GPS site velocity with respect to stable Nubia (4 mm yr⁻¹ 95% confidence)

Figure 1

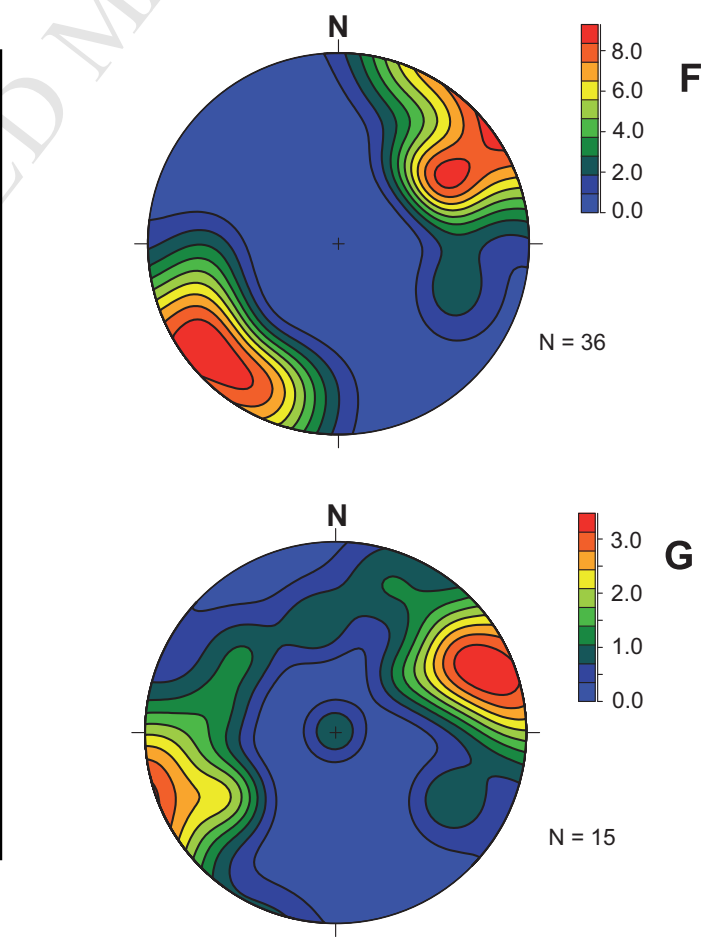
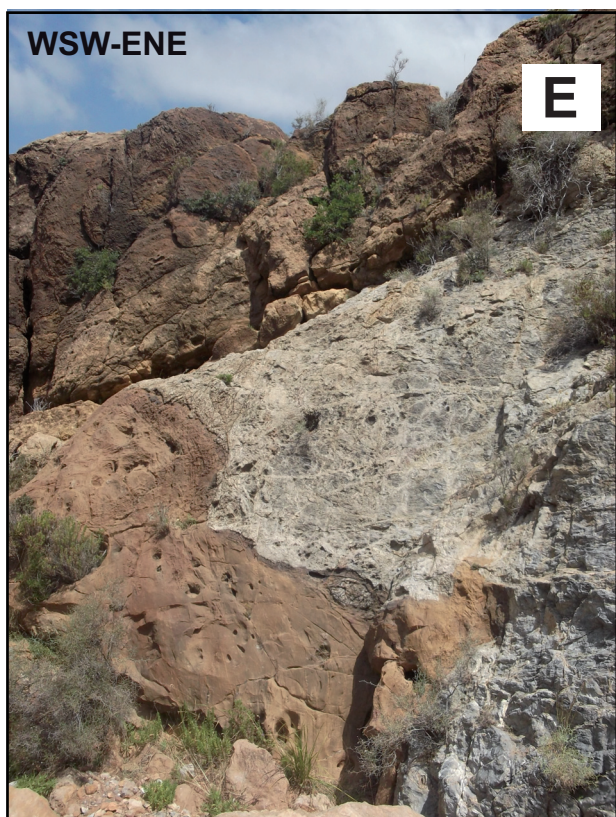
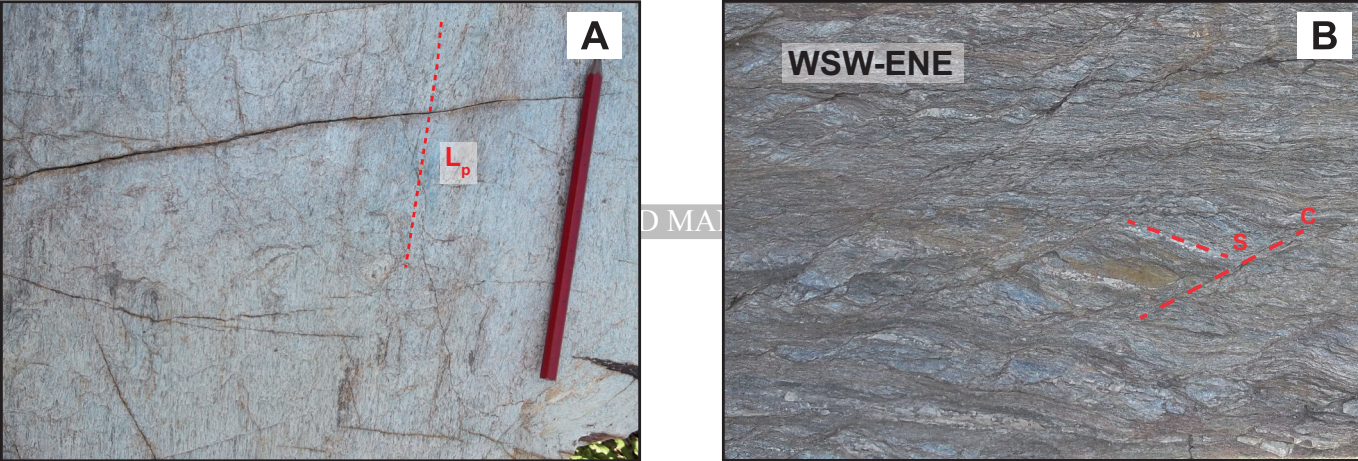


Figure 10

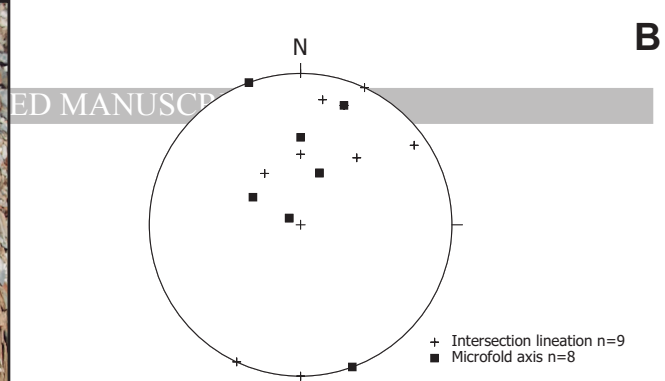
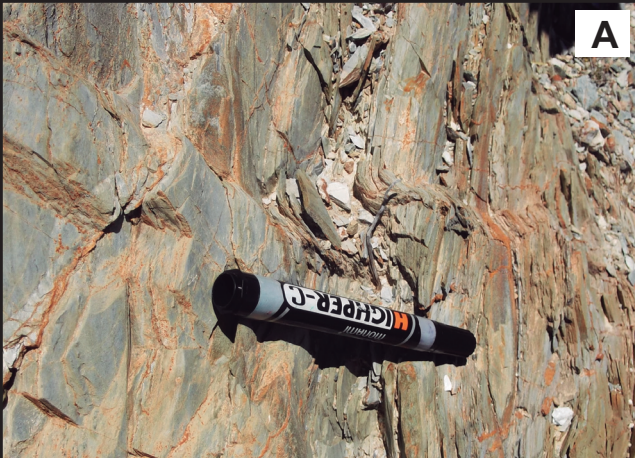


Figure 11

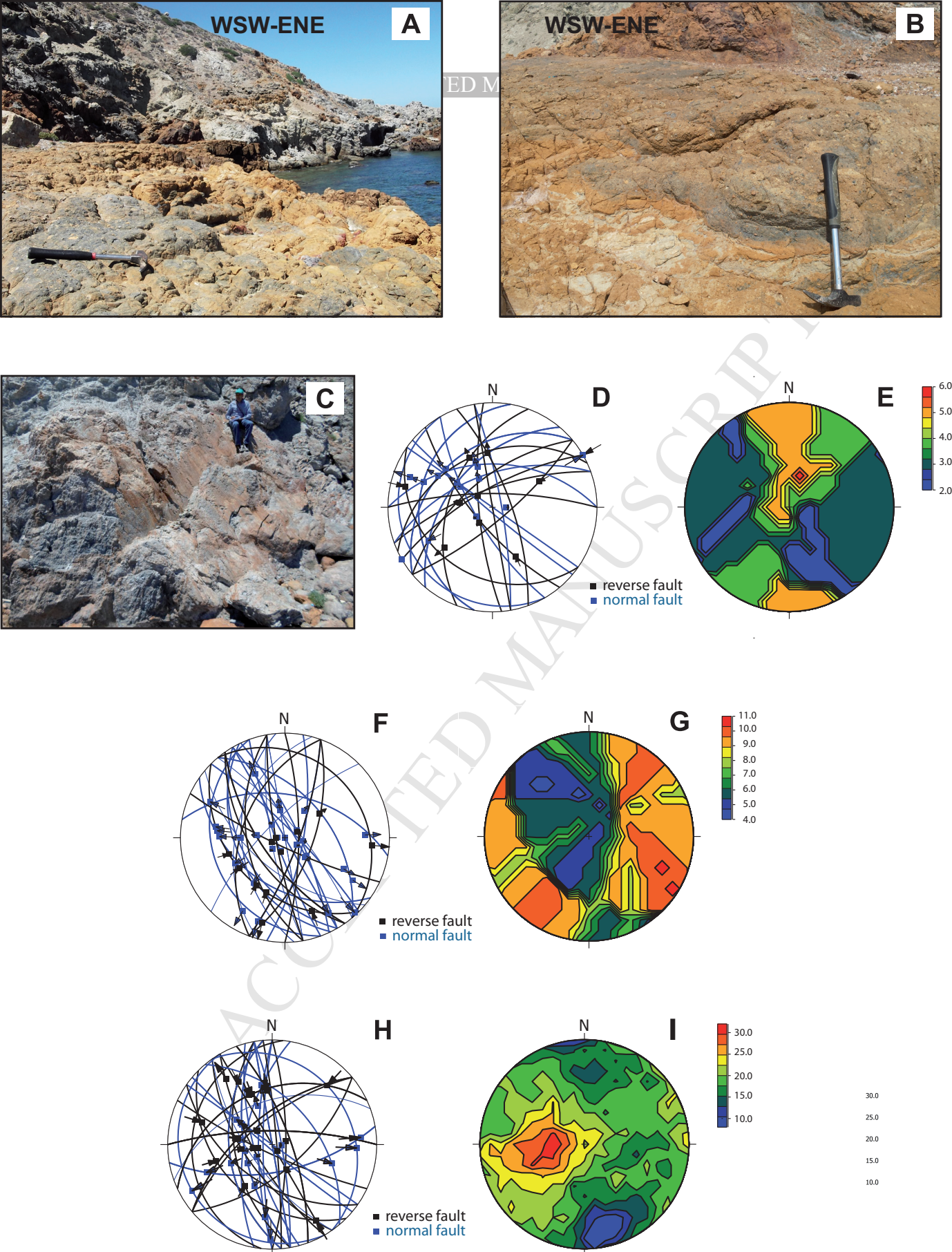


Figure 12

A

ACTIVE SECTION OF THE
TEMSAMANE DETACHMENT
E-W Hanging wall movement according
GPS site velocity
 $\approx 4 \text{ mm yr}^{-1}$

INACTIVE SECTION OF THE
TEMSAMANE DETACHEMNT
E-W Footwall movement according
GPS site velocity
 $\approx 0 \text{ mm yr}^{-1}$

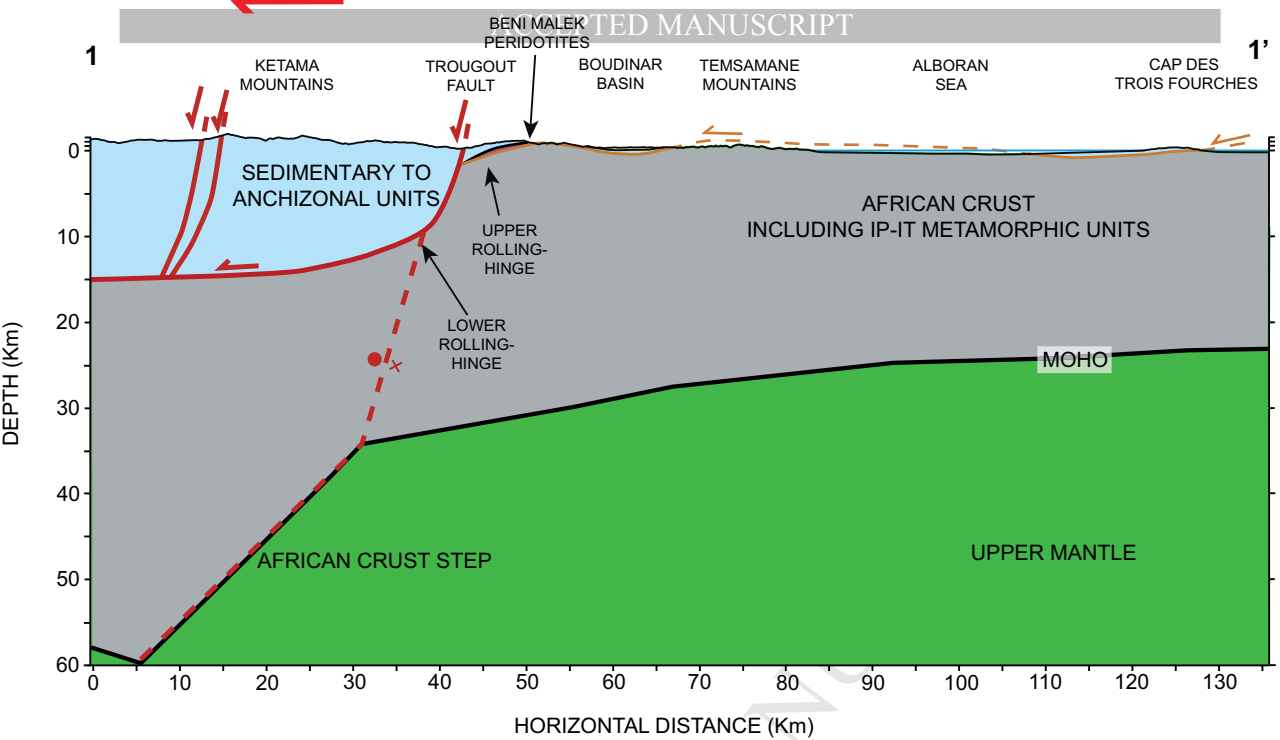
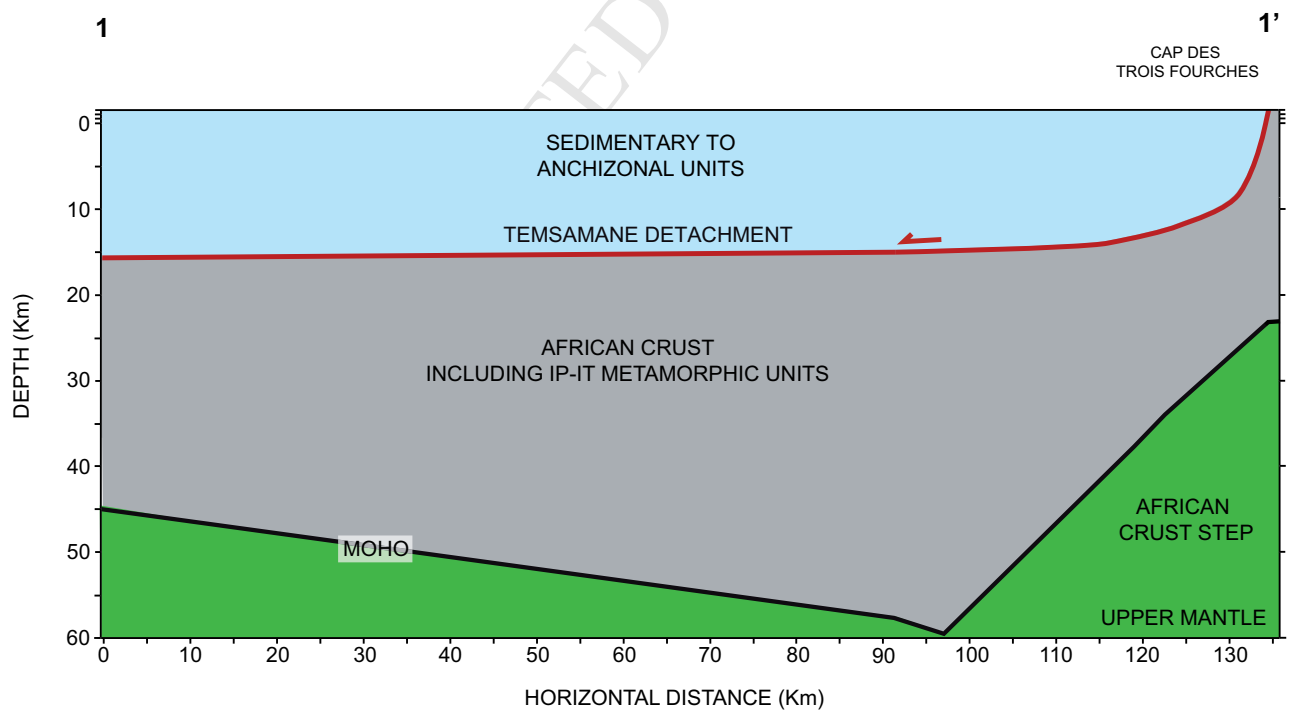
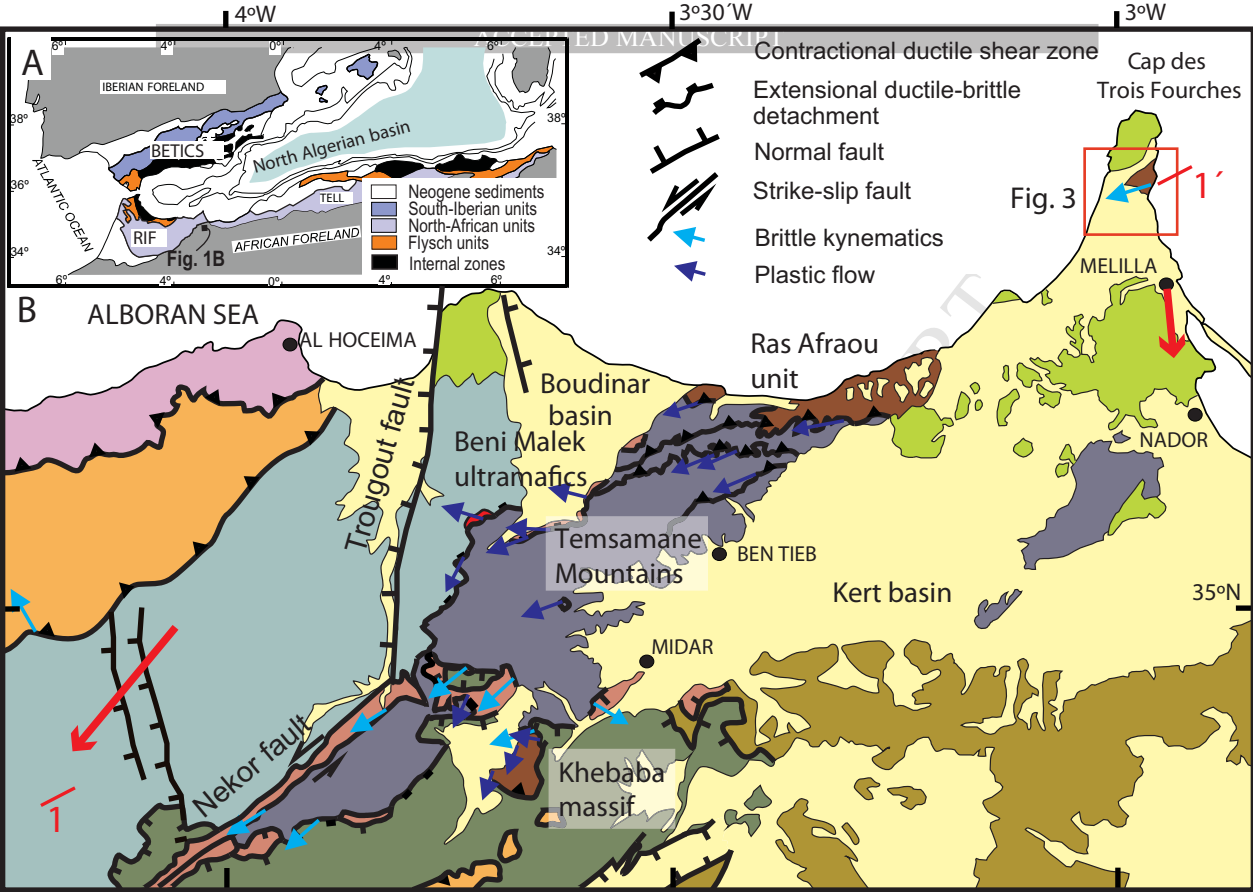
**B**

Figure 13



North African paleomargin

- [Green] Aknoul unit, Cretaceous shales
- [Light Blue] Tanger-Ketama unit, Jurassic marbles
- [Light Blue] and Cretaceous slates, with
 - (a) Beni Malek peridotites
- [Brown] Paleozoic chloritoid-bearing schists
- [Red] Paleozoic to Jurassic greenschist rocks, mostly mylonitic
- [Dark Blue] Temsamane greenschist units
- [Yellow] Rifean foreland units (Gareb) and Middle Atlas



GPS site velocity
4 mm yr⁻¹ 95% confidence

Internal Rif or Alborán Domain

- [Pink] Dorsal and Ghomaride units
- [Orange] Cretaceous to Burdigalian turbidites
- [Yellow] Late Neogene-Quaternary sediments
- [Green] Late Neogene volcanics

Maghrebian Flyschs

Cretaceous to Burdigalian turbidites

Intermontane basins

Late Neogene-Quaternary sediments

Late Neogene volcanics

Figure 2

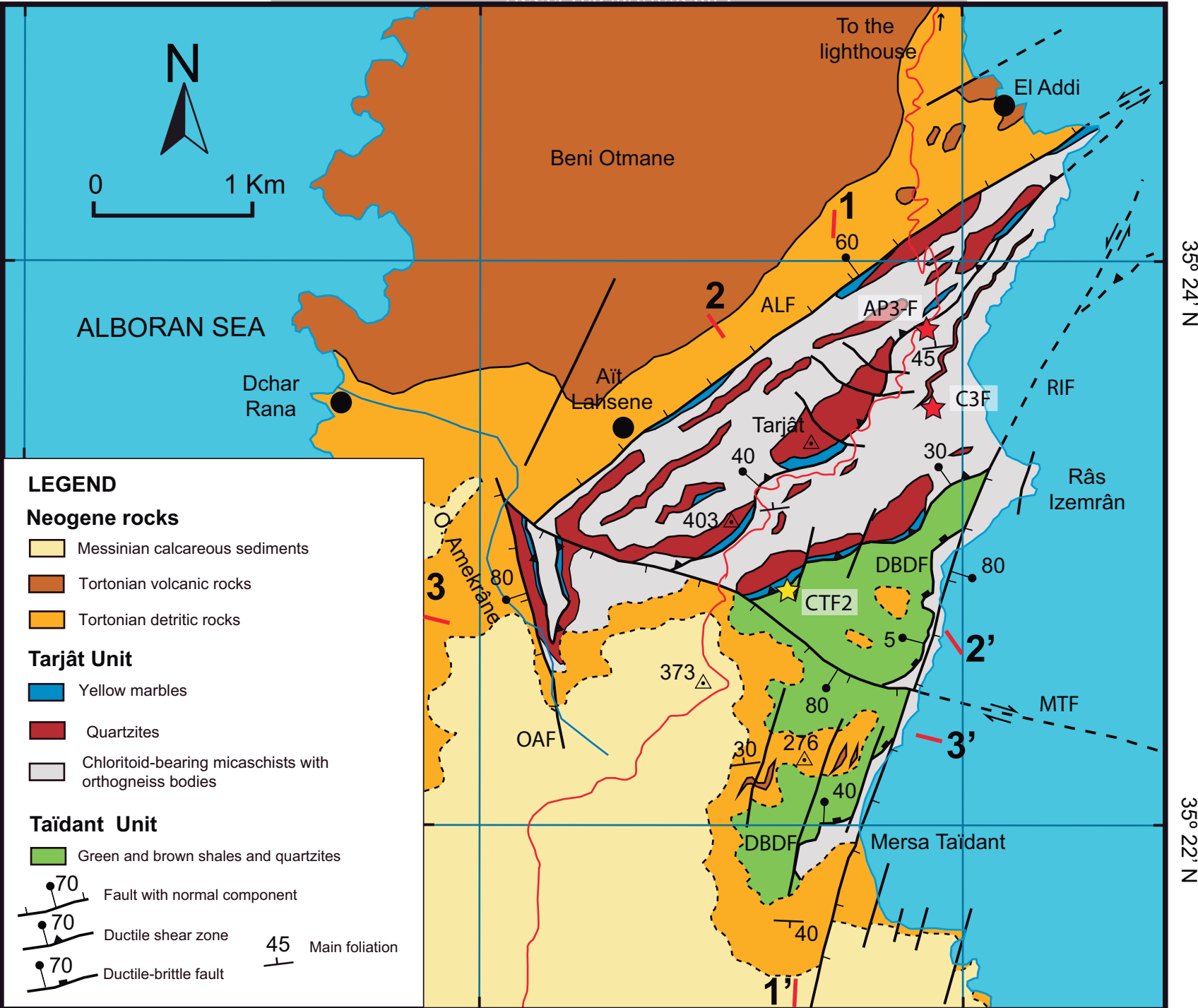


Figure 3

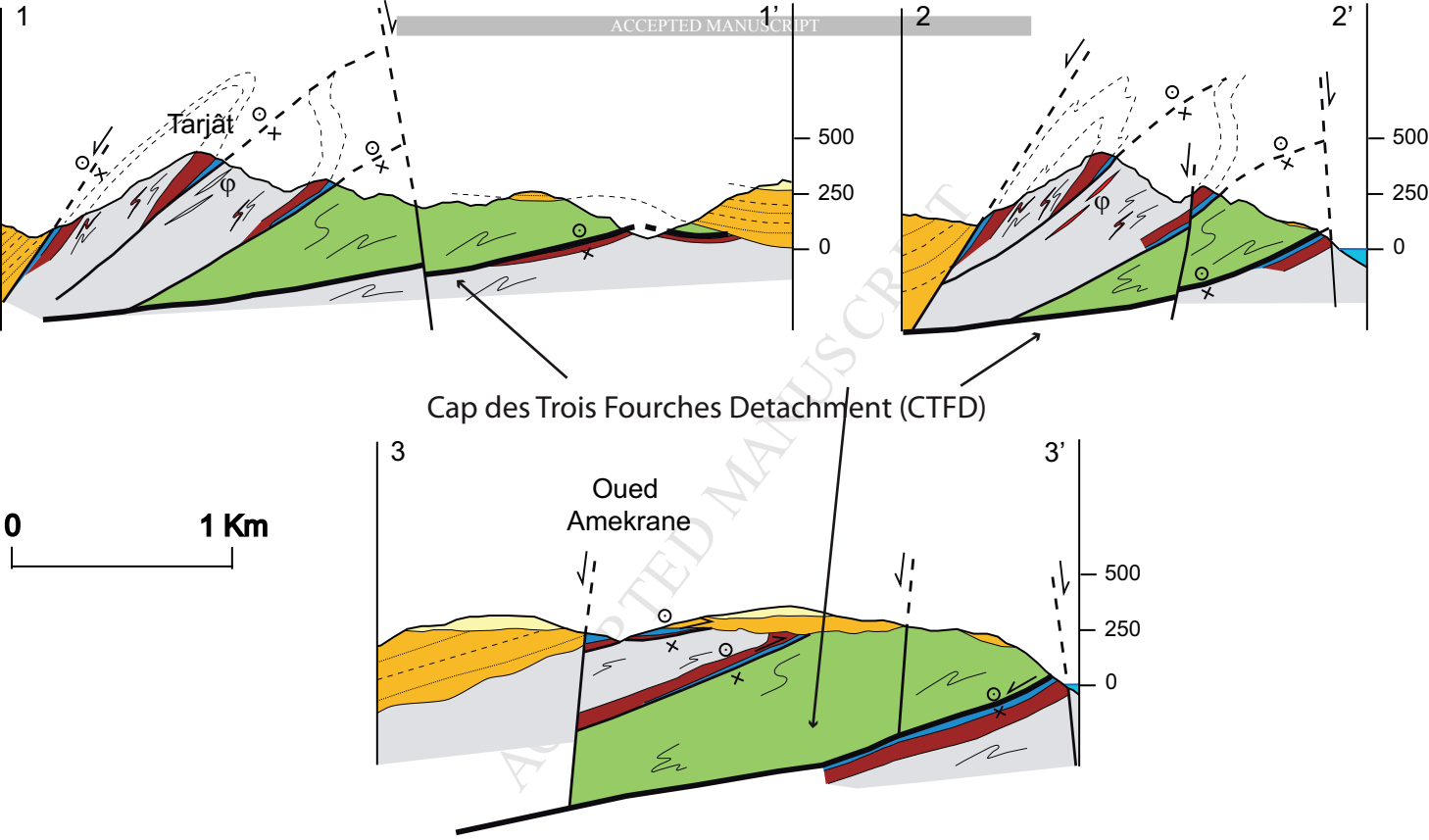


Figure 4

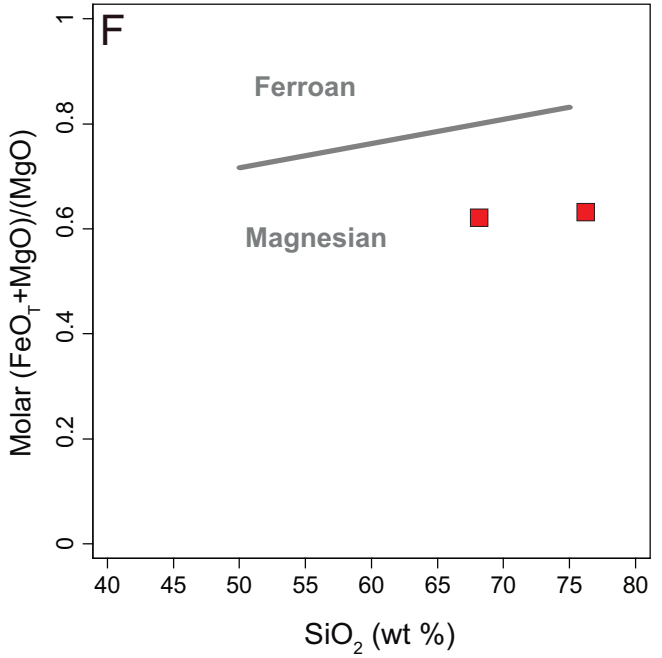
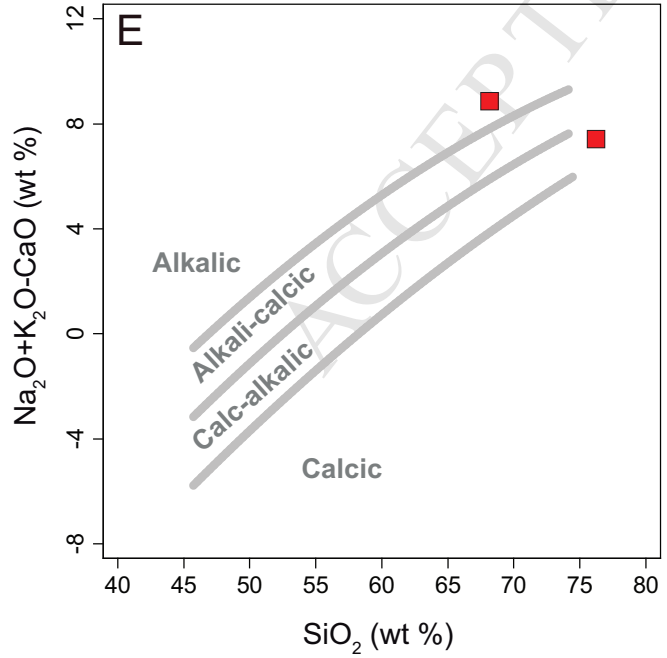
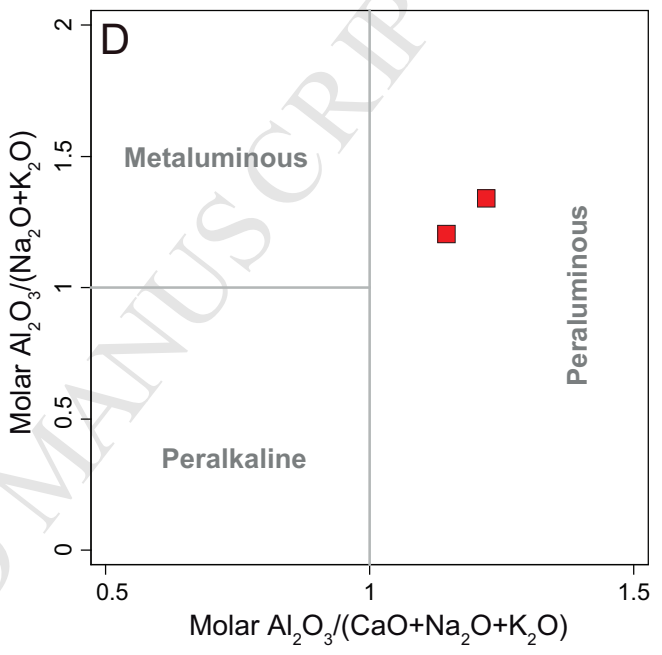
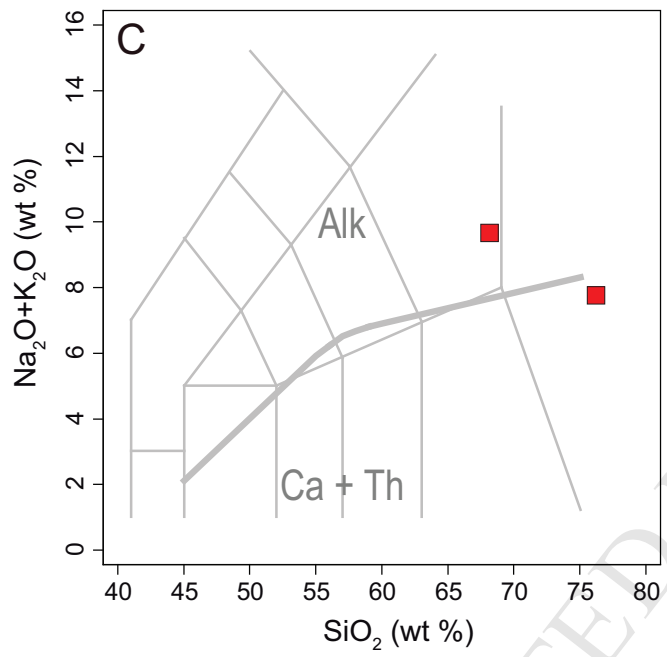
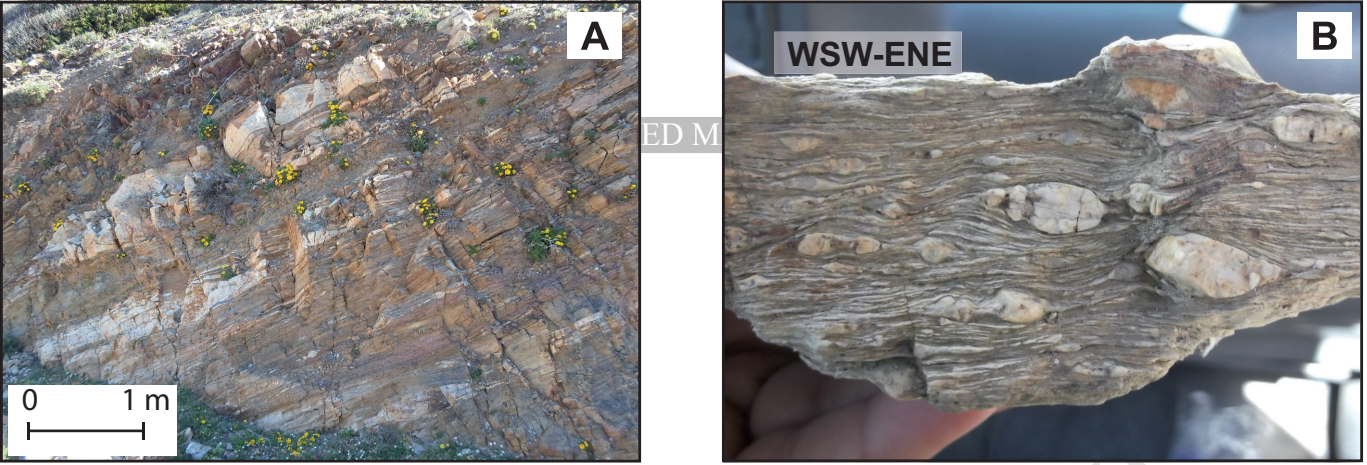
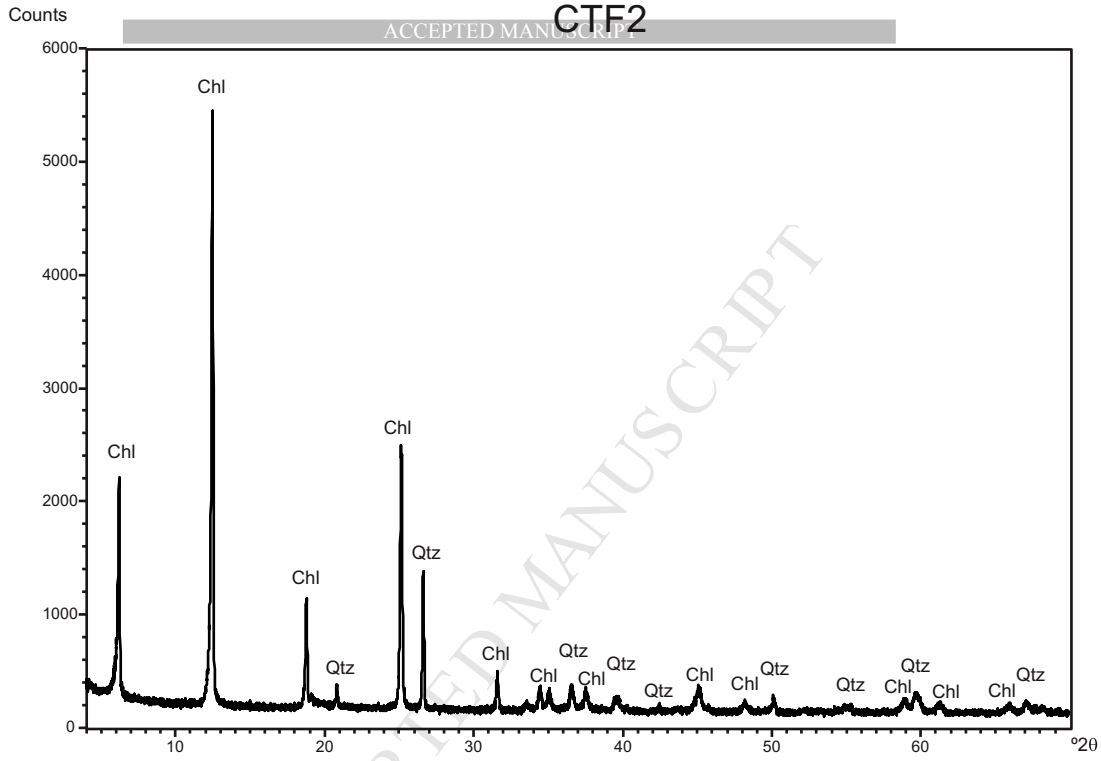
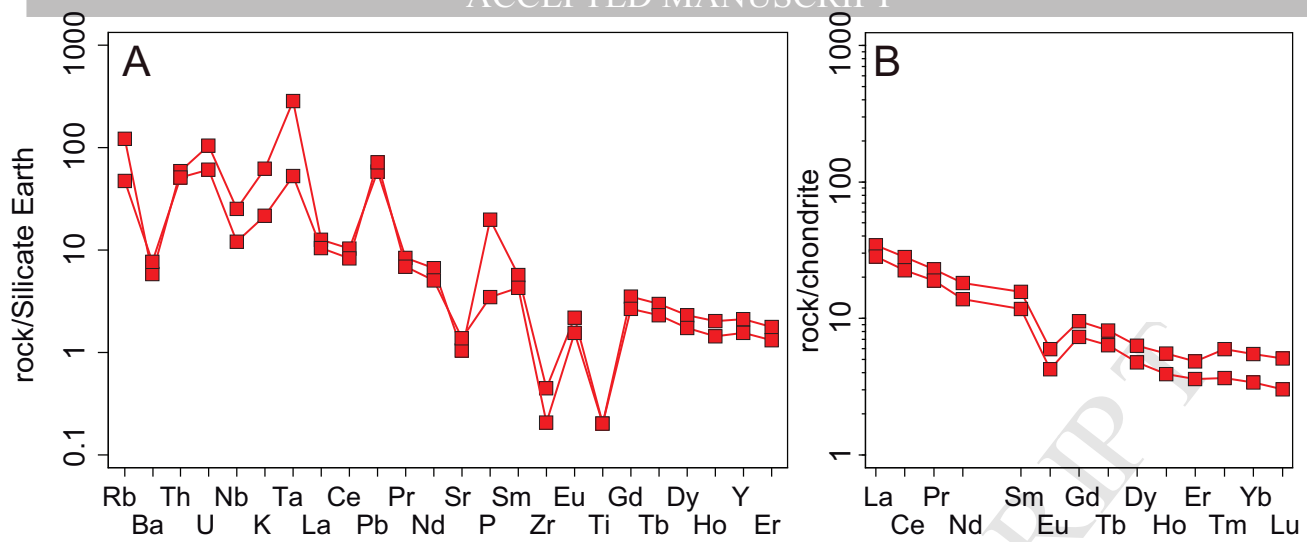


Figure 5

**Figure 6**

**Figure 7**

Wetherhill plot, Common-lead uncorrected

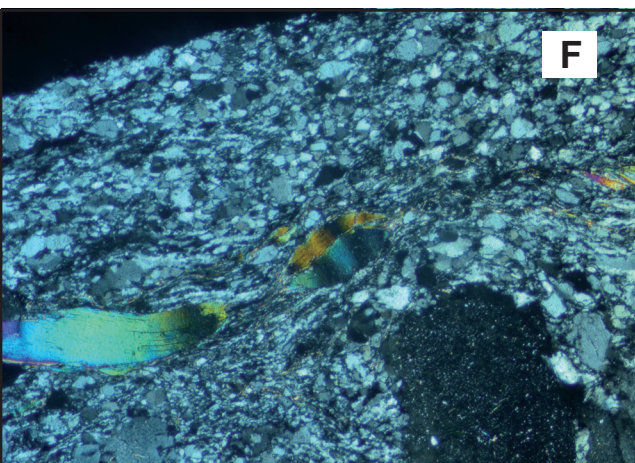
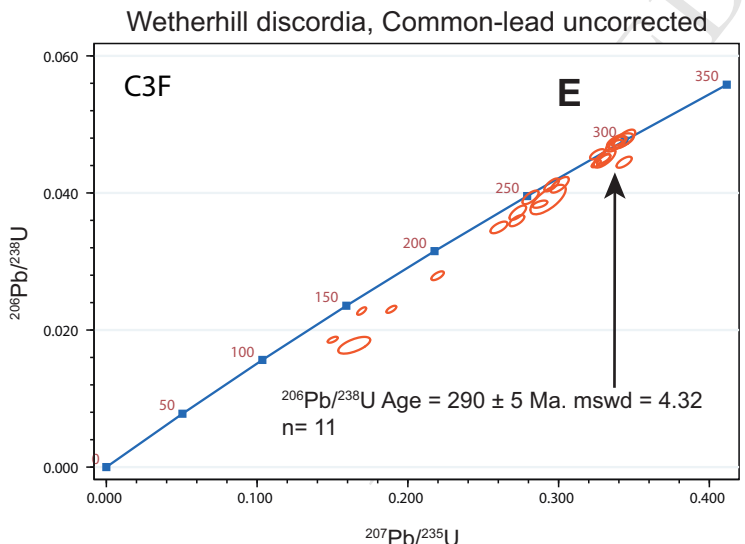
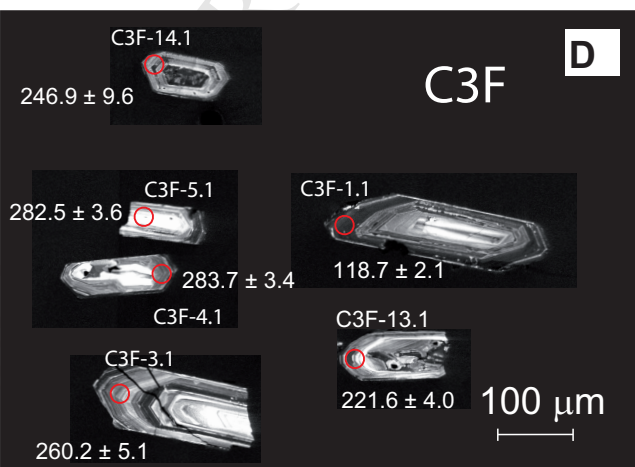
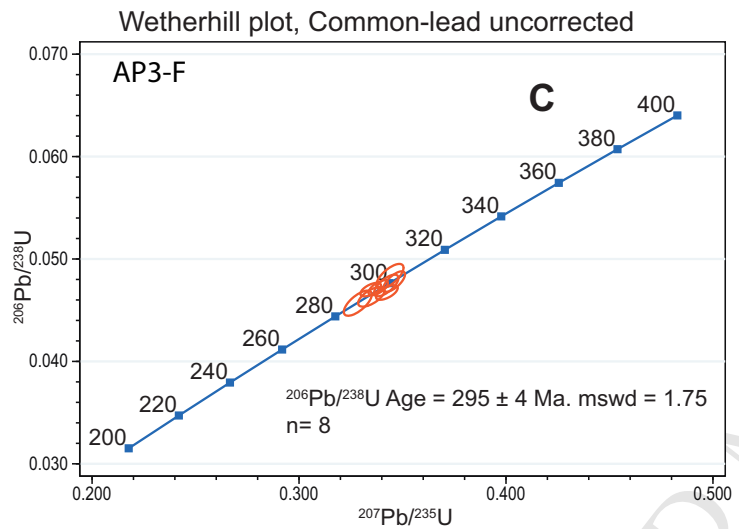
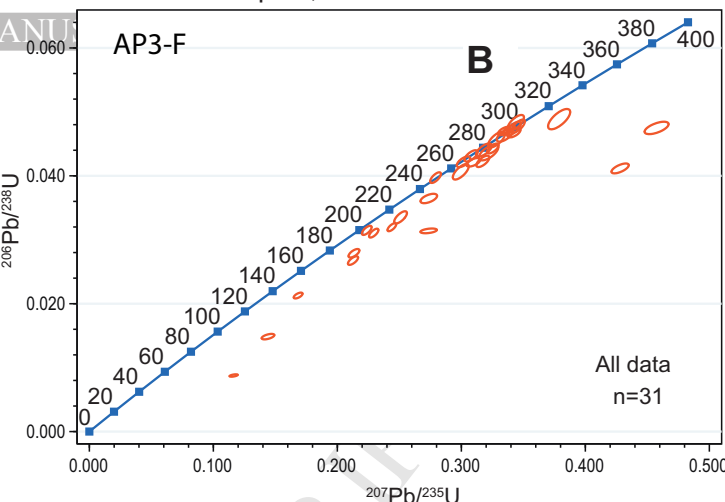
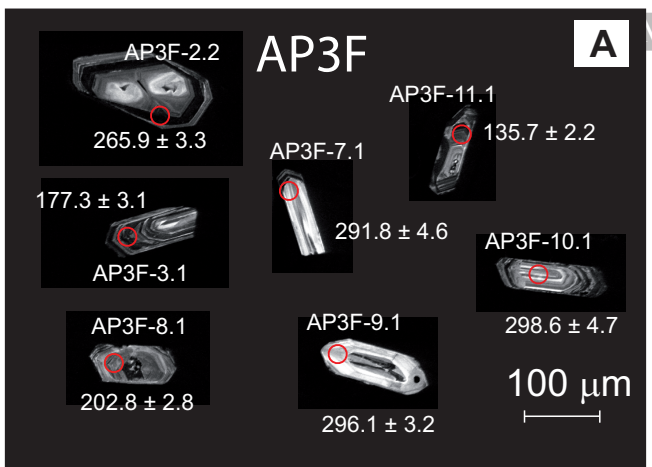


Figure 8

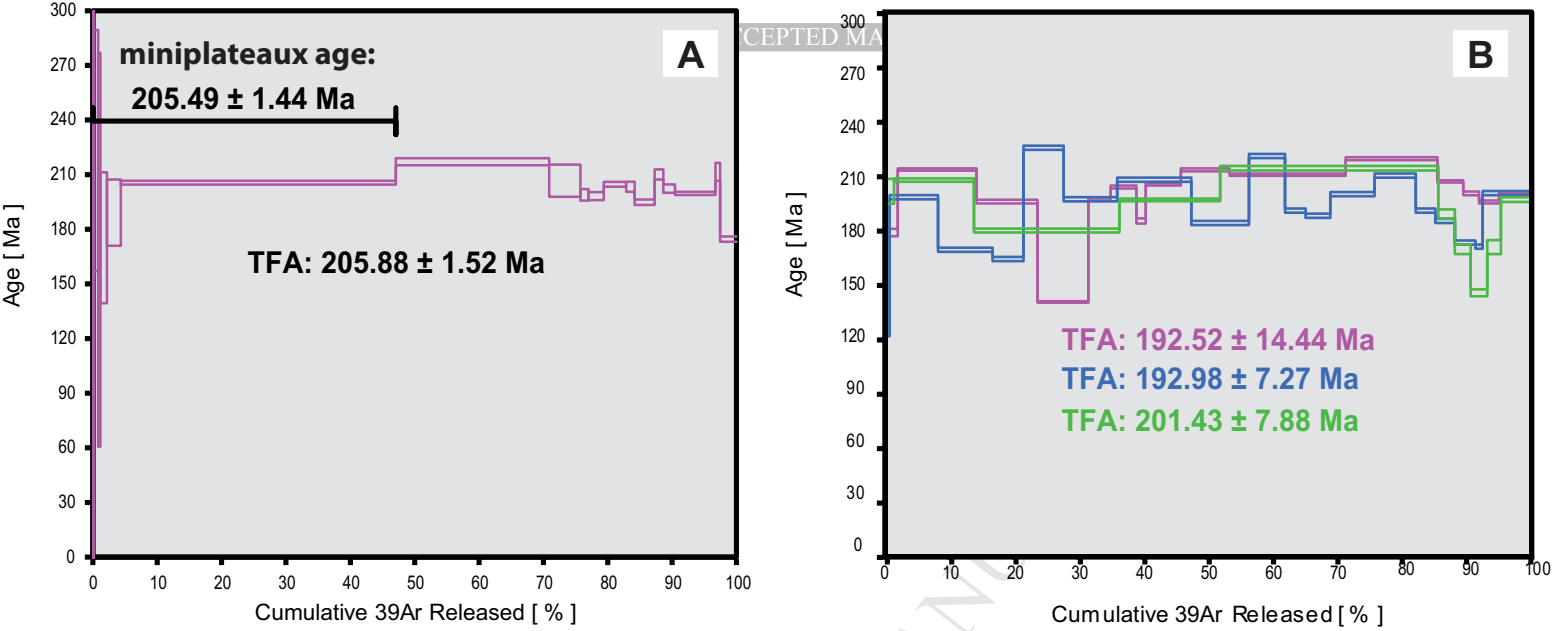


Figure 9

ACCEPTED MANUSCRIPT

We determined the structure of the Cap des Trois Fourches area

We describe, for the first time, the orthogneisses in the area ages

U-Pb SHRIMP zircon geochronology yield early Permian ages for their protoliths

We propose a model of the crustal structure